



OPEN ACCESS

EDITED BY

Xiao-Ping Xia,
Chinese Academy of Sciences (CAS), China

REVIEWED BY

A. Ramachandran,
V.O. Chidambaram College, India
Douaa Fathy,
Minia University, Egypt
H. M. Zakir Hossain,
Jashore University of Science and
Technology, Bangladesh

*CORRESPONDENCE

Qian Hou,
✉ houqianhj@126.com

RECEIVED 08 November 2023

ACCEPTED 04 March 2024

PUBLISHED 08 April 2024

CITATION

Xia Y, Hou Q and Mou C (2024), Geochemistry of siltstones in the North Qilian Zhongbao–Mayinggou formations (Late Ordovician–Early Silurian): implications for paleoclimate, paleoweathering, and tectonic setting.
Front. Earth Sci. 12:1334982.
doi: 10.3389/feart.2024.1334982

COPYRIGHT

© 2024 Xia, Hou and Mou. This is an open-access article distributed under the terms of the [Creative Commons Attribution License \(CC BY\)](https://creativecommons.org/licenses/by/4.0/). The use, distribution or reproduction in other forums is permitted, provided the original author(s) and the copyright owner(s) are credited and that the original publication in this journal is cited, in accordance with accepted academic practice. No use, distribution or reproduction is permitted which does not comply with these terms.

Geochemistry of siltstones in the North Qilian Zhongbao–Mayinggou formations (Late Ordovician–Early Silurian): implications for paleoclimate, paleoweathering, and tectonic setting

Yu Xia^{1,2,3}, Qian Hou^{2,3*} and Chuanlong Mou^{1,2,3}

¹Shandong University of Science and Technology, Qingdao, China, ²Chengdu Center, China Geological Survey (Geosciences Innovation Center of Southwest China), Chengdu, China, ³Key Laboratory for Sedimentary Basin and Oil and Gas Resources, Ministry of Natural Resources, Chengdu, China

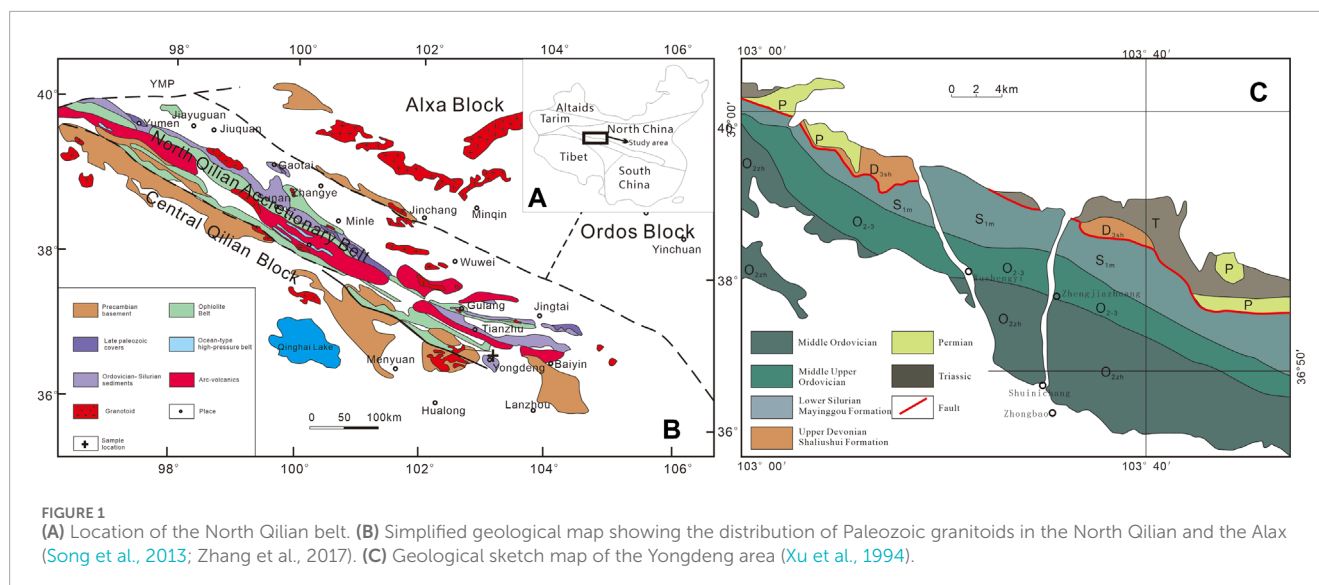
The Late Ordovician–Early Silurian period witnessed the Phanerozoic mass extinction, glacial events, and volcanic events. Paleoweathering indexes chemical index of alteration (CIA), chemical index of weathering (CIW), and plagioclase index of alteration (PIA) indicated that the source area weathering changed from weak to moderate to intense. CIA values in the upper Zhongbao formation ranged from 66.71% to 73.97%, indicating a drier and colder climate. Upward, the CIA values on the bottom of the Mayinggou formation returned to the high value quickly (from 73.86% to 81.31%), suggesting that the ice age ended, the climate became warmer and wetter, and the sea level rose. The Al_2O_3 –(CaO^* + Na_2O)– K_2O triangular plots, Hf–La/Th, and SiO_2 – $\text{Al}_2\text{O}_3/\text{TiO}_2$ bivariate plots inferred that the source of the siltstones in the two formations is mostly from the felsic igneous rocks. The samples from the Zhongbao–Mayinggou formations have chondrite-normalized rare earth element (REE) patterns similar to that of the North Qilian volcanic arc rocks. Geochemical discrimination plots displayed that the sediments of the Zhongbao–Mayinggou formations came from the active continental margin setting.

KEYWORDS

clastic sediment geochemistry, Ordovician–Silurian, sedimentary rocks, tectonic setting, provenance, paleoweathering

1 Introduction

The Late Ordovician–Early Silurian transition was an important part of Earth's history, which was marked by the Gondwanan glaciation, extinction of life, global environmental change, extensive volcanism, and massive plate movement (Melchin et al., 2013; Ran et al., 2015; Zhou et al., 2015; Algeo et al., 2016). However, most of the research studies



about these amazing events are about the stable blocks, while there are few research studies about the orogenic belts (Ran et al., 2015; Ge et al., 2019; Lei et al., 2019; Men et al., 2022). At the end of the Ordovician, there was evidence of glaciation, which proves the ice sheet in the region of the Gondwana (Paris et al., 1995; Ghienne, 2003). On the basis of faunal, geochemical, and lithological analysis results from the South China Late Ordovician–Early Silurian boundary strata, scholars (Rong and Chen, 1987; Chen et al., 2004; Fan et al., 2009; Mou et al., 2020) indicated that a brief glaciation existed. According to a series of geochemical features (Zhang et al., 2000; Yan et al., 2010; Zhou et al., 2015; Zou et al., 2018), scholars considered those oceanic fluctuations from pneumatorexis to oxygenated to hypoxic water columns and climatic changes from warming to cooling to warming in the Upper Ordovician–Lower Silurian. All the above studies were carried out in the Yangtze area, which is consistent with the Hirnantian glaciation in the Gondwanan area. Because of the complicated geological conditions, the North Qilian orogenic belt Ordovician–Silurian strata are poorly exposed and discontinuous. The North Qilian Orogen strata of the Hirnantian to Rhuddanian interval have been named the Zhongbao and Mayinggou formations (Du et al., 2006; Bai et al., 2016). The Shihuigou section is located in the North Qilian Orogen; successive Zhongbao–Mayinggou formations (Hou et al., 2021), fresh samples, and exact geochemical date have been obtained to conduct research on the clastic rocks of the Zhongbao and Mayinggou formations. So, it is a suitable section to conduct research on the climatic variation in the North Qilian belt in the Upper Ordovician–Lower Silurian transitional stratum.

The temporal relationship between the glaciation and the ocean anoxia is notably a controversial topic. By evaluating the mineralogical, petrological, and the geochemical characteristics of clastic rocks during the Late Ordovician–Early Silurian transition period, this paper provides a new understanding of the paleoclimate, provenance, redox conditions, and paleoenvironmental changes during the important Ordovician–Silurian period. The aim is to find evidence that this glacial period also had an effect on the orogenic belt.

2 Geological setting

From the Late Ordovician to the Early Silurian, the North Qilian orogenic belt lay on the northern margin of Gondwana (Li et al., 2017a, b). In the Early Paleozoic, the North Qilian Ocean was located between the Central Qilian block and the Arax block (Zhang et al., 2015; Figure 1A). The southern part of the North Qilian orogenic belt is cut by the middle Qilian fault. The northern Qilian belt is cut off by the Zuolangnanshan fault. The North Qilian orogenic belt is part of the Central orogenic belt of China (Zheng et al., 2010; Dong and Santosh, 2016). The North Qilian orogenic belt is characterized by ophiolite belts, granite belts, arc-shaped accretionary wedges, and some basic structural units from north to south (Zuo and Wu, 1997; Xia et al., 2003; Song et al., 2009).

The Shihuigou section [SHP 36°51' 29" N, 103°13' 35" E] is the first named location of the Ordovician Zhongbao formation in Yongdeng County, Gansu Province, China. It is located in the eastern part of the North Qilian belt (Figure 1B). The strata crossing the Upper Ordovician–Lower Silurian boundary in the Yongdeng section are Zhongbao and Mayinggou formations (Figure 2). Their ages are well constrained by the biostratigraphic date and the basalt date (Feng, 1992; Xia et al., 1996; Xia et al., 2003; Xu et al., 2003). The Zhongbao formation is composed of clastic rock, chert, volcanic rock, and carbonate rock. The overlying Mayinggou Formation is composed of mudstone and clastic rock (Figure 2) (Hou et al., 2018a; b, 2021). The deposition of the Late Ordovician was mainly affected by volcanic ash events and the tectonic collision, and the tectonic setting was a multi-island deep-water basin (Hou et al., 2021).

3 Samples and methodology

A total of 35 clastic sediment samples were collected from Zhongbao and Mayinggou formations in the Shihuigou section (Figure 2). We removed the calcite vein and cleaned the surface soil of all samples. In addition, all samples were packed into

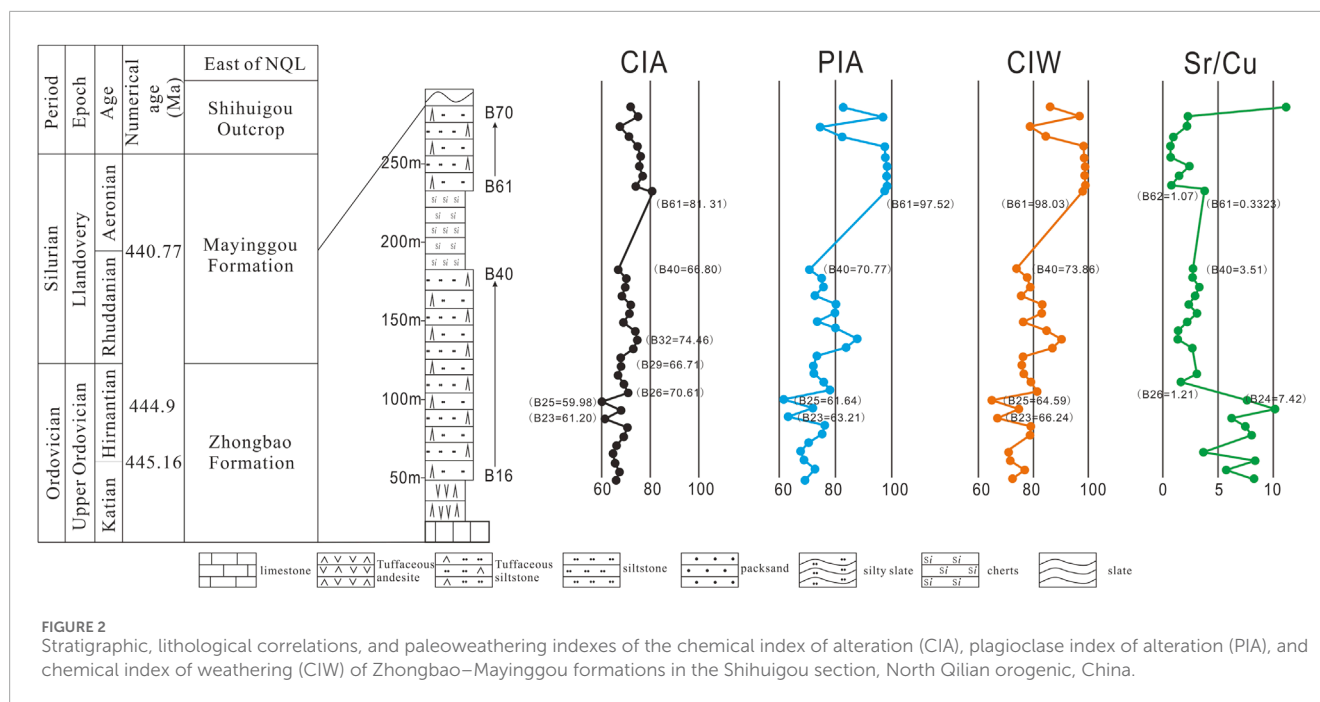


FIGURE 2

Stratigraphic, lithological correlations, and paleoweathering indexes of the chemical index of alteration (CIA), plagioclase index of alteration (PIA), and chemical index of weathering (CIW) of Zhongbao–Mayinggou formations in the Shihuigou section, North Qilian orogenic, China.

plastic bags to prevent contamination and oxidation as much as possible. Analysis of major elements, trace elements, and rare earth elements (REEs) was carried out in the key laboratory of Beijing Institute of Uranium Geology, China National Nuclear Corporation. Detrital samples were crushed and ground in an agate mortar to less than 200 mesh for geochemical analysis. The main elements were analyzed using an X-ray fluorescence spectrometer (PW2404). The analysis uncertainty is generally less than 2%. The loss on ignition (LOI) of the sample was calculated by heating at 1,000°C for 90 min, and the weight loss was recorded. Thirty-five trace elements (including rare earth elements) in 20 clastic samples were analyzed using an inductively coupled plasma mass spectrometer (ICP-MS), according to Chinese National Standard DZ/T 0223-2001 (2001). The analysis process is described below. First, the powder (25 mg) was digested in a high-pressure resistant beaker containing a mixture of hydrofluoric acid (HF)–nitric acid (HNO₃) (1:1), heated at 80°C for 36 h, and evaporated. The solution was then evaporated until dry, and 1.5 mL HF, 1.5 mL HNO₃, and 0.5 mL HClO₄ were added. The beaker containing the solution was then covered and digested in an oven at 190°C for at least 48 h. Finally, the solution was diluted to 50 mL with 1% HNO₃ for analysis. Trace elements were determined using the Thermo Scientific ELEMENT XRICP-MS instrument at 20°C and 30% relative humidity. The analysis uncertainty is generally less than 5%.

4 Results

4.1 Petrology

In total, 34 siltstone samples and 1 chert sample were selected from Zhongbao and Mayinggou formations in the Shihuigou section for thin-section analyses. In O_{2-3z} (Zhongbao Formation) and S_{1m} (Mayinggou Formation) siltstone, the thin section shows that the

mineral constituent of this outcrop consisted of clay minerals, quartz, and few micas (Figure 3). The color of outcrop siltstone is celadon. The bed thickness varies from 6 cm to 30 cm, but most are between 20 and 25 cm thick. The siltstone layer is fresh and has a typical pyroclastic structure without a sedimentary structure. The siltstones are composed of quartz (30%–60%) and clay mineral (40%–60%). The quartz grains have mostly subangular shapes and sizes between 50 and 450 μm.

4.2 Geochemistry

4.2.1 Major element characteristics

Concentrations of major elements in samples from the Zhongbao–Mayinggou formations are listed in Table 1. For the siltstones in the Zhongbao Formation, SiO₂ (55.37%–77.68%) and Al₂O₃ (8.41%–17.12%) are the most abundant oxides. The content of chemical components in the study sample is compared with post-Archean average shale (PAAS) values (Table 1). The comparison shows that the clastic sediments of the Zhongbao Formation had low SiO₂ content, which was similar to that in Paleozoic greywacke (66.1%). However, it is significantly lower than typical feldspar (77.1%) and quartz sandstone (91.5%) (Fedo et al., 1995; Cullers and Podkovyrov, 2000). The main elements of the Zhongbao Formation changed little and were relatively stable. Most samples had high contents of K₂O (1.41%–4.17%, average = 2.16%) and Al₂O₃ (8.41%–17.12%, average = 13.09%), suggesting the high content of clay mineral. The content of Fe₂O₃^T, TiO₂, and MgO is negatively correlated with the content of SiO₂, which indicated that the unstable component content in the sandstones in the siltstones decreases gradually with the increase in maturity of sandstone.

The content of SiO₂ in of the Mayinggou Formation clastic samples ranges from 71.08% to 90.95%; the average content of the sample chemical constituents is compared with the PAAS values

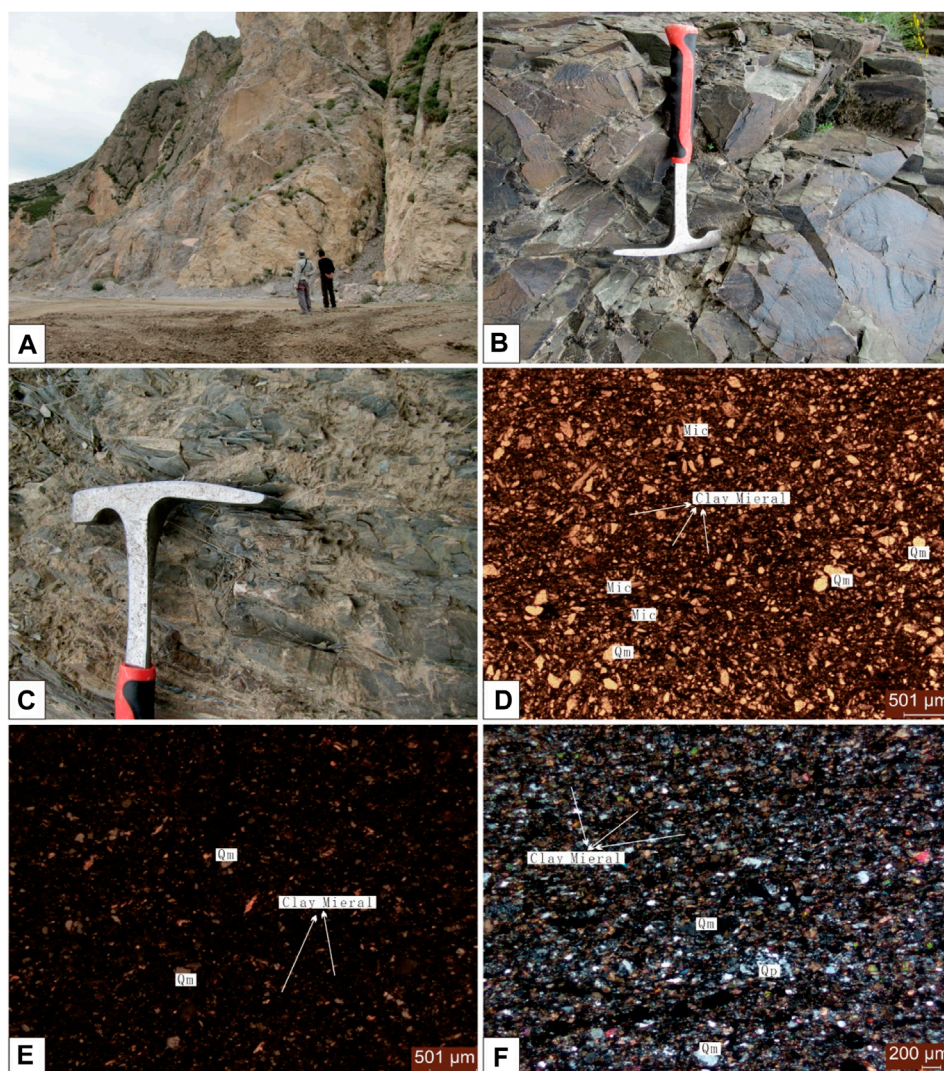


FIGURE 3 Macrophotographs and photomicrographs of the siltstone texture in Shihuigou sections from the Zhongbao and Mayinggou formations. (A–C) Macroscopic characteristics of siltstones. (D–F) Microscopic characteristics of siltstones. Qm, monocrystalline quartz; Qp, polycrystalline.

(Table 1). The comparison showed that the sedimentary rocks of the Mayinggou Formation had high SiO_2 content, which was between typical arkose (77.1%) and quartz sandstone (91.5%). Most samples had low contents of K_2O (1.18%–3.36%, average = 1.78%) and Al_2O_3 (4.2%–11.79%, average = 6.56%), suggesting the small content of clay mineral.

4.2.2 Trace elements

The trace element data on siltstones from Zhongbao–Mayinggou formations are listed in Table 2 and show the trace element distribution in silt sandstone treated with post-Archean Australian shale (PAAS) normalization (Taylor and McLennan, 1985). Compared with PAAS, the siltstones from Zhongbao and Mayinggou formations are highly depleted in Ni, Cu, Sr, Rb, Zr, Co, V, and Cr contents and slightly depleted in Ba, U, Zn, Sc, and thorium (Th) contents.

Ba is the most abundant trace element (501.08 ppm on average) in the siltstone samples of the Zhongbao Formation. The average content of Sr was 156.93 ppm, which is the second abundant trace element. The Mayinggou Formation siltstone samples also contain high concentrations of Ba (average 544.14 ppm). The Sr content in Mayinggou Formation siltstone samples is lower than that in the Zhongbao Formation (average 46.17 ppm). The average contents of Ni, Co, Th, Cu, Rb, V, Zr, Sc, and Cr in siltstone samples are 30.44, 14.06, 11.98, 37.63, 86.68, 77.18, 57.66, 11.76, 71.39, 11.98, and 37.63 ppm, respectively. The concentrations of niobium (Nb) and thorium in siltstones are mainly continental and insoluble in seawater (Kato et al., 2002). So, the concentrations of these elements in the siltstone indicate the extent of the influence of terrigenous materials. Th and Nb concentrations were positively correlated with terrigenous primary elements TiO_2 and Al_2O_3 (Figure 4).

TABLE 1 Concentrations of major elements in clastic rock from the Shihuigou section, North Qilian belt.

Sample	SiO ₂	Al ₂ O ₃	Fe ₂ O ₃	MgO	CaO	Na ₂ O	K ₂ O	MnO	TiO ₂	P ₂ O ₅	Loss on ignition (LOI)	FeO	Chemical index of alteration of alteration (CIA)	Plagioclase index of alteration (PIA)	Chemical index of weathering (CIW)
SHP-B16	71.06	12.14	4.4	2.09	1.6	3.03	1.66	0.05	0.56	0.15	3.16	3.87	65.87	69.36	72.39
SHP-B17	67.88	13.66	5.32	2.56	1.62	2.5	2.54	0.05	0.62	0.16	3.09	4.7	67.22	72.97	76.83
SHP-B18	71.01	11.86	5.01	2.38	1.56	3.13	1.51	0.07	0.63	0.16	2.68	3.99	65.67	68.82	71.66
SHP-B19	70.75	11.86	4.82	2.3	1.94	3.01	1.55	0.08	0.62	0.15	2.81	3.85	64.6	67.56	70.55
SHP-B20	70.41	12.31	4.93	2.39	1.38	2.95	1.99	0.06	0.62	0.16	2.76	3.85	66.08	70.44	73.98
SHP-B21	69.15	13.23	5.05	2.53	1.15	2.42	2.35	0.06	0.58	0.16	3.22	3.53	69.09	75.29	78.75
SHP-B22	70.4	13.13	5.01	2.33	0.67	2.8	1.99	0.04	0.61	0.16	2.79	3.49	70.61	76.23	79.08
SHP-B23	69.57	11.35	4.39	2.11	3.19	3.04	1.41	0.11	0.53	0.14	4.15	3.24	61.2	63.21	66.24
SHP-B24	71.31	12.36	4.64	2.26	1.13	3.05	1.64	0.05	0.58	0.15	2.74	3.29	67.99	71.95	74.73
SHP-B25	55.78	10.17	3.81	1.79	12.29	2.93	1.21	0.26	0.62	0.18	10.93	3.1	59.98	61.64	64.59
SHP-B26	61.17	16.69	7.04	3.47	0.94	2.88	3	0.09	0.78	0.2	3.68	5.83	71	78.2	81.39
SHP-B27	63.87	10.95	4.51	2.71	5.55	1.49	2.04	0.06	0.65	0.18	7.89	3.35	69.19	75.86	79.43
SHP-B28	55.37	8.41	3.05	1.75	14.4	1.37	1.59	0.2	0.42	0.11	13.29	2.19	66.71	72.34	76.33
SHP-B29	77.68	11.26	2.44	1.26	0.33	3.32	1.65	0.02	0.24	0.06	1.71	1.9	67.99	72.46	75.51
SHP-B30	66.89	13.72	5.26	2.65	1.59	2.6	2.31	0.06	0.67	0.17	4.02	3.9	67.85	73.14	76.61
SHP-B31	61.43	17.12	6.65	3.39	0.67	1.91	3.73	0.06	0.77	0.18	4.01	4.42	73.06	83.83	86.89
SHP-B32	58.84	18.14	7.9	3.74	0.47	1.49	4.17	0.09	0.77	0.18	4.13	6.77	74.76	87.72	90.27
SHP-B33	65.42	14.13	6.66	3.69	0.81	1.72	2.44	0.05	0.78	0.21	3.98	4.47	73.97	82.19	84.8
SHP-B34	69.16	12.19	5.22	3.08	1.56	2.22	1.71	0.05	0.64	0.16	3.93	4.02	68.95	73.49	76.33

(Continued on the following page)

TABLE 1 (Continued) Concentrations of major elements in clastic rock from the Shihuigou section, North Qilian belt.

Sample	SiO ₂	Al ₂ O ₃	Fe ₂ O ₃	MgO	CaO	Na ₂ O	K ₂ O	MnO	TiO ₂	P ₂ O ₅	Loss on ignition (LOI)	FeO	Chemical index of alteration (CIA)	Plagioclase index of alteration (PIA)	Chemical index of weathering (CIW)
SHP-B35	59.37	15.3	6.78	4.1	2.19	1.64	2.98	0.15	0.76	0.19	6.47	5	71.49	79.79	83.06
SHP-B36	59.81	15.07	6.63	3.91	2.66	1.59	2.82	0.09	0.76	0.19	6.45	4.66	72.05	80.19	83.28
SHP-B37	67.58	14.17	5.1	2.28	1.5	3.08	1.99	0.08	0.69	0.18	3.31	3.35	68.32	72.67	75.57
SHP-B38	65.52	13.54	5.9	3.61	1.72	1.9	2.26	0.1	0.7	0.17	4.55	3.99	69.74	75.72	78.92
SHP-B39	67.59	12.53	6.14	3.5	1.41	2.16	1.74	0.04	0.69	0.17	3.97	4.42	70.24	75.14	77.83
SHP-B40	67.49	11.94	5.48	3.17	2.47	2.22	1.71	0.06	0.66	0.18	4.59	3.84	66.8	70.77	73.86
SHP-B61	78.01	6.72	8.32	1.22	0.41	0.07	1.41	0.33	0.27	0.09	3.14	3.48	81.31	97.52	98.03
SHP-B62	83.81	7.12	2.52	0.94	0.37	0.04	2.4	0.14	0.28	0.07	2.28	0.82	74.18	98.37	98.92
SHP-B63	86.61	5.33	2.63	0.88	0.37	0.04	1.52	0.2	0.24	0.03	2.13	0.86	77.02	98.19	98.7
SHP-B64	87.66	5.44	2.21	0.93	0.09	0.03	1.69	0.07	0.21	0.03	1.64	1.11	75.65	98.4	98.89
SHP-B65	90.95	4.28	1.25	0.51	0.11	0.04	1.27	0.04	0.19	0.03	1.31	0.59	76.15	97.71	98.38
SHP-B66	75.73	10.52	4.64	1.86	0.17	0.1	3.36	0.14	0.47	0.05	2.87	3.14	74.82	97.54	98.31
SHP-B67	86.79	5.01	2.34	1.12	0.78	0.43	1.21	0.11	0.16	0.03	2	1.81	71.26	82.42	86.07
SHP-B68	71.08	11.79	4.5	2.38	1.34	1.84	2.5	0.2	0.55	0.26	3.55	3.25	67.49	74.5	78.76
SHP-B69	83.82	4.2	2.11	0.96	3.18	0.05	1.3	0.19	0.12	0.03	3.9	1.59	75.09	96.88	97.83
SHP-B70	86.71	5.17	2.05	1.36	0.68	0.44	1.18	0.13	0.16	0.04	2.04	1.41	71.99	82.75	86.14
PAAS	62.8	18.9	7.2		1.3	1.2	3.7	2.2	1	0.16					

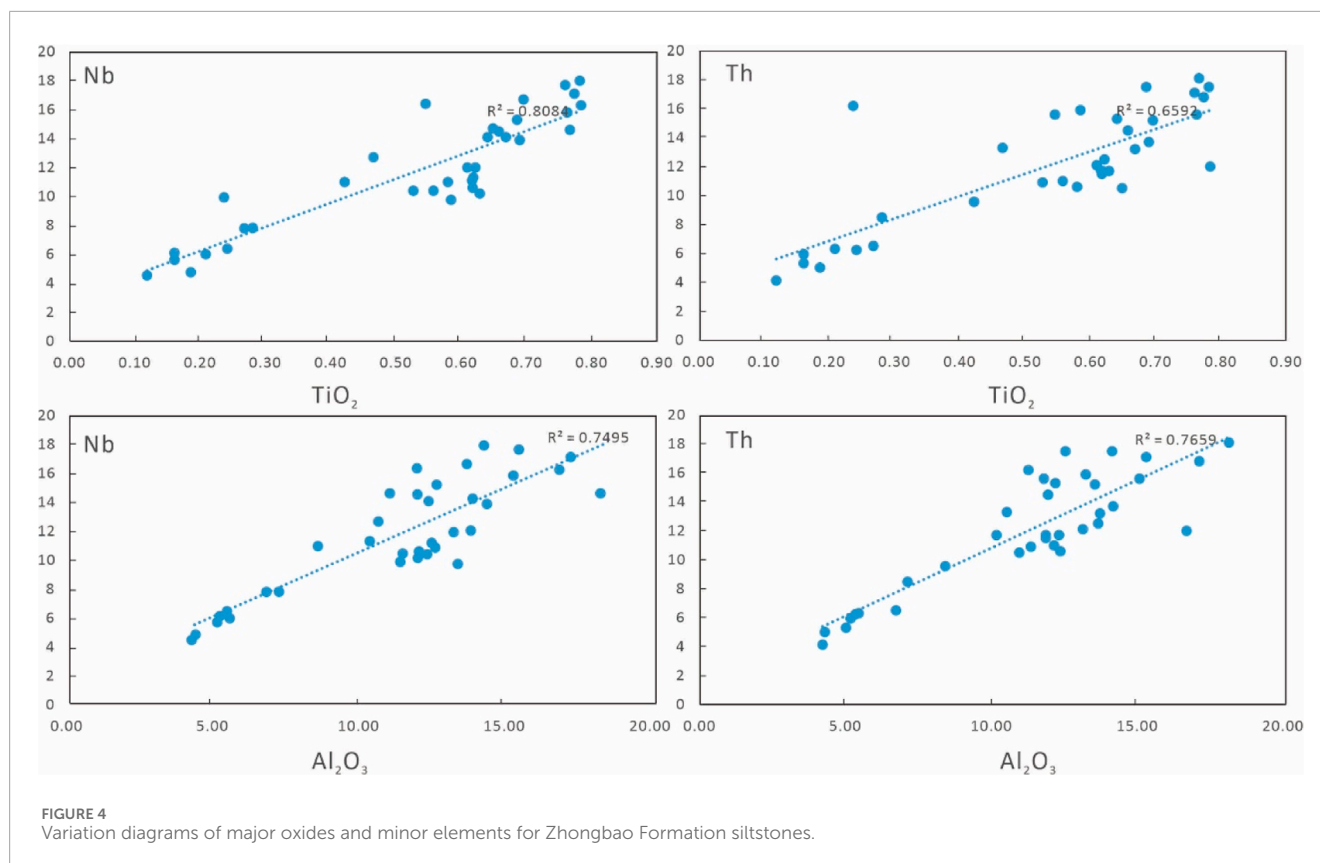
TABLE 2 Concentrations of trace elements in clastic rock from the Shihuigou section, North Qilian belt.

Sample	Li	Be	Sc	V	Cr	Co	Ni	Cu	Zn	Ga	Rb	Sr	Y	Cs	Ba	Pb	Th	U	Nb	Ta	Zr	Hf	Th/Sc	Th/Co	La/Sc	Cr/Th
SHP-B16	19.00	1.15	11.10	73.90	72.00	12.30	21.50	22.50	63.00	13.60	61.30	183.00	20.20	2.51	485.00	18.50	11.00	1.92	10.40	0.80	65.90	3.71	0.99	0.89	27.04	6.55
SHP-B17	23.20	1.75	13.90	86.60	84.10	16.60	28.10	30.50	62.60	15.80	113.00	169.00	24.70	4.64	781.00	13.80	12.50	2.41	12.00	0.94	70.90	4.27	0.90	0.75	19.94	6.73
SHP-B18	22.30	1.48	13.50	88.60	99.10	15.10	23.20	23.50	70.60	13.30	58.00	194.00	23.40	2.26	616.00	20.90	11.70	2.06	10.20	0.78	70.60	4.54	0.87	0.77	21.08	8.47
SHP-B19	24.20	1.31	12.80	90.80	98.30	14.60	29.60	58.30	80.20	14.70	63.10	195.00	23.60	3.14	448.00	20.70	11.50	2.20	10.60	0.81	69.90	4.46	0.90	0.79	25.11	8.55
SHP-B20	22.60	1.32	13.10	80.90	85.30	15.00	23.80	24.30	70.80	14.30	65.20	195.00	23.70	3.15	717.00	18.40	11.70	2.17	11.10	0.81	65.70	4.35	0.89	0.78	26.97	7.29
SHP-B21	22.40	1.83	12.50	77.40	74.40	14.20	25.20	24.30	68.50	17.00	112.00	178.00	19.00	4.02	531.00	19.10	15.90	2.93	9.76	1.04	59.20	3.82	1.27	1.12	15.25	4.68
SHP-B22	28.00	1.54	11.50	81.20	79.50	13.60	24.20	23.00	60.60	15.50	77.70	140.00	26.20	3.87	454.00	7.49	12.10	2.37	12.00	0.92	67.30	4.14	1.05	0.89	24.35	6.57
SHP-B23	20.30	0.87	11.20	69.80	70.90	12.40	24.30	21.90	63.20	12.20	60.70	223.00	20.70	3.27	334.00	17.20	10.90	2.08	10.40	0.75	64.30	4.13	0.97	0.88	37.24	6.50
SHP-B24	22.10	1.22	11.80	76.60	76.40	12.60	21.80	23.30	73.10	13.50	53.60	173.00	16.70	3.54	385.00	18.10	10.60	2.32	11.00	0.83	67.90	4.47	0.90	0.84	22.54	7.21
SHP-B25	18.80	1.02	10.70	80.10	74.50	11.40	34.30	19.80	61.60	11.90	50.30	388.00	29.00	2.71	319.00	14.70	11.70	1.97	11.30	0.82	75.20	4.68	1.09	1.03	33.82	6.37
SHP-B26	39.50	2.78	18.10	125.00	112.00	22.30	41.90	88.00	116.00	23.60	79.40	111.00	30.00	4.76	711.00	20.70	12.00	2.82	16.30	1.26	77.80	4.63	0.66	0.54	11.33	9.33
SHP-B27	25.00	1.60	9.69	69.30	72.00	10.70	29.60	61.70	86.20	13.90	51.90	169.00	24.60	3.12	394.00	17.40	10.50	2.92	14.70	1.21	76.20	4.68	1.08	0.98	24.63	6.86
SHP-B28	18.40	1.04	7.67	47.30	37.80	8.40	29.30	13.50	46.60	10.60	65.50	372.00	30.40	2.90	277.00	13.70	9.57	2.36	11.00	0.77	52.30	3.28	1.25	1.14	31.54	3.95
SHP-B29	12.00	1.36	5.94	25.80	20.40	5.25	7.78	10.90	34.50	10.10	68.30	225.00	24.00	3.09	398.00	24.90	16.20	3.22	9.94	0.97	44.00	3.25	2.73	3.09	19.26	1.26
SHP-B30	29.20	1.76	14.80	96.30	88.10	15.70	31.80	64.10	89.50	16.70	98.70	143.00	29.10	5.17	503.00	14.90	13.20	2.68	14.10	1.08	73.00	4.67	0.89	0.84	21.31	6.67
SHP-B31	37.80	2.80	20.20	141.00	105.00	20.30	41.70	86.30	115.00	25.60	165.00	81.50	29.90	8.53	827.00	14.70	16.80	2.85	17.10	1.39	73.00	4.97	0.83	0.83	11.57	6.25
SHP-B32	37.50	2.79	22.70	128.00	100.00	23.40	40.80	55.70	115.00	23.30	174.00	56.40	28.30	12.10	791.00	29.80	18.10	3.14	14.60	1.19	70.30	4.38	0.80	0.77	13.15	5.52
SHP-B33	36.70	1.90	17.10	104.00	119.00	20.10	44.20	30.90	94.80	16.70	108.00	57.20	25.70	6.42	395.00	20.50	17.50	3.46	18.00	1.45	74.80	5.34	1.02	0.87	23.11	6.80
SHP-B34	30.90	1.26	12.70	79.60	96.30	16.00	35.20	27.30	74.30	13.80	72.60	76.10	23.30	3.72	322.00	30.40	15.30	2.79	14.10	1.07	71.70	4.54	1.20	0.96	27.30	6.29
SHP-B35	48.10	2.46	19.40	114.00	114.00	23.70	80.80	83.60	107.00	21.90	142.00	163.00	28.50	6.88	624.00	23.50	17.10	3.95	17.70	1.38	80.20	5.14	0.88	0.72	18.78	6.67
SHP-B36	44.20	1.99	18.70	114.00	108.00	19.80	46.30	35.60	103.00	19.20	124.00	92.00	26.60	6.90	563.00	22.80	15.60	3.12	15.80	1.24	66.20	4.74	0.83	0.79	21.31	6.92
SHP-B37	35.80	1.44	14.90	88.40	93.40	13.50	27.70	33.20	79.70	15.10	87.70	99.70	24.10	4.51	490.00	15.90	13.70	2.66	13.90	1.03	68.40	4.50	0.92	1.01	27.01	6.82

(Continued on the following page)

TABLE 2 (Continued) Concentrations of trace elements in clastic rock from the Shihuigou section, North Qilian belt.

Sample	Li	Be	Sc	V	Cr	Co	Ni	Cu	Zn	Ga	Rb	Sr	Y	Cs	Ba	Pb	Th	U	Nb	Ta	Zr	Hf	Th/Sc	Th/Co	La/Sc	Cr/Th	
SHP-B38	42.00	1.63	14.50	100.00	118.00	16.00	45.70	32.10	90.40	15.70	103.00	75.70	24.80	6.14	446.00	23.60	15.20	3.10	16.70	1.23	66.80	4.53	1.05	0.95	22.39	7.76	
SHP-B39	46.60	1.80	12.70	93.30	128.00	15.70	35.20	27.30	88.30	14.40	97.30	65.50	23.00	5.28	309.00	20.20	17.50	3.79	15.30	1.11	69.00	4.29	1.38	1.11	21.11	7.31	
SHP-B40	36.50	1.63	12.90	106.00	120.00	15.90	38.60	28.00	80.00	15.30	83.00	98.30	27.50	5.07	407.00	21.30	14.50	3.14	14.50	1.22	69.00	4.11	1.12	0.91	22.82	8.28	
SHP-B61	25.00	1.49	7.41	53.80	26.40	14.90	56.10	67.10	401.00	10.40	61.50	22.30	22.20	2.54	507.00	111.00	6.51	2.24	7.79	0.61	22.80	2.56	0.88	0.44	15.23	4.06	
SHP-B62	14.40	1.69	10.30	67.30	35.00	29.70	68.10	103.00	78.70	10.70	105.00	111.00	17.10	4.83	928.00	29.80	8.48	4.30	7.82	0.60	22.60	1.47	0.82	0.29	12.37	4.13	
SHP-B63	12.90	1.16	6.15	31.00	25.70	10.30	23.50	11.90	61.00	8.33	67.80	24.50	10.10	3.54	1,894.00	4.63	6.24	1.86	6.38	0.45	17.50	1.25	1.01	0.61	12.93	4.12	
SHP-B64	10.10	1.24	6.16	31.00	22.50	7.46	12.50	28.70	40.70	8.54	80.00	7.95	7.47	3.02	448.00	19.80	6.31	3.56	6.00	0.42	18.20	1.11	1.02	0.85	10.81	3.57	
SHP-B65	13.10	1.07	4.93	29.50	23.30	9.38	10.60	33.50	31.70	6.50	57.20	8.08	6.85	2.38	357.00	14.40	5.02	1.03	4.76	0.36	14.20	0.90	1.02	0.54	8.02	4.64	
SHP-B66	30.30	1.84	11.20	90.70	56.60	15.40	18.90	26.40	74.70	14.20	147.00	14.00	13.30	7.78	821.00	15.00	13.30	1.30	12.70	0.93	32.60	2.18	1.19	0.86	17.66	4.26	
SHP-B67	13.20	0.92	4.56	29.20	14.60	5.25	9.05	21.30	32.70	7.65	54.80	38.90	6.25	2.82	271.00	10.60	5.31	2.01	5.61	0.41	19.90	1.15	1.16	1.01	16.58	2.75	
SHP-B68	28.60	1.91	8.77	66.60	15.60	7.12	12.90	40.20	76.40	15.40	115.00	77.00	14.80	6.08	618.00	18.40	15.60	2.85	16.40	0.95	121.00	6.03	1.78	2.19	19.01	1.00	
SHP-B69	16.40	1.11	4.03	28.60	12.60	3.51	10.80	12.20	23.50	7.10	61.40	137.00	5.98	2.59	295.00	12.30	4.13	1.40	4.54	0.33	14.40	0.93	1.02	1.18	10.45	3.05	
SHP-B70	16.10	1.05	4.10	35.80	19.90	4.45	10.50	23.00	30.90	7.44	48.70	21.00	7.74	2.43	422.00	69.40	5.95	3.81	6.10	0.40	21.90	1.24	1.45	1.34	11.81	3.34	
PAAS			16	150	110	23	55	50	85		160	200			650												



4.2.3 Rare earth element

The analysis dates of REEs are shown in Table 3, and the normalized model of chondrites is shown in Figure 5. All samples are normalized to chondritic values, and the distribution curves of rare earth elements are similar. The calculation of Eu anomalies follows that performed by Rollinson (1993), $Eu/Eu^* = (EuN)/[(SmN \times GdN)^{1/2}]$, where the subscript N represents the normalization of rare earth elements to chondritic values (Taylor and McLennan, 1985). The samples of the Zhongbao Formation are enriched in light rare earth elements (LREEs), the heavy rare earth element (HREE) pattern is relatively flat, and the Eu anomaly is negative. The samples of the Mayinggou Formation also showed that the LREE was enriched and the heavy REE pattern was relatively flat, but the HREE and LREE values were lower than those of the Zhongbao group.

The total content of rare earth elements (ΣREE) in the Zhongbao Formation showed remarkable variability (126.99–203.57 ppm, average = 160.79 ppm) (Table 3), which was significantly lower than the value in the PAAS standard (184.77 ppm) (Taylor and McLennan, 1985).

The light rare earth element values ranged from 110.79 to 182.66 ppm, with an average of 143.72 ppm. The HREE content was 12.35–21.5 ppm, with an average value of 17.06 ppm. The average LREE/HREE ratio was 8.42, with a range of 7.1–9.64. The (LaN/YbN) ratio ranges from 6.23 to 10.29, with an average value of 8.68. The Eu/Eu^* values showed a negative anomaly overall, with an average Eu/Eu^* value of 0.68 and

a range of 0.47–0.83, which is significantly higher than the value of PAAS.

The range of ΣREE in the Mayinggou Formation was 45.34–156.94 ppm, with an average value of 87.86 ppm. The content of LREEs (40.65–143.89 ppm, average 79.36 ppm) was significantly higher than that of HREEs (4.6–15.27 ppm, average 8.4 ppm). It is like the distribution of rare earth elements in shale (Ketris and Yudovich, 2009). The LREE/HREE ratio ranged from 6.43 to 12.44, with an average of 9.45. The LaN/YbN ratio varies from 6.39 to 11.59, with an average of 9.66. The siltstone has no negative Eu anomaly, and the fluctuation range is 0.58–1.33 (average 0.73).

5 Discussion

5.1 Paleoweathering indexes and paleoclimate implications

Enhanced chemical weathering under wet conditions leads to leaching out of alkali metals and alkali metal elements (Na, Ca, and K). On the other hand, the content of Si and Al in the residue is increased (Akarish and El-Gohary, 2008; Moosavirad et al., 2011). Among different weathering indexes, the most commonly used ancient weathering indexes to evaluate the degree of chemical weathering in the source area are the chemical index of alteration (CIA) (Nesbitt and Young, 1982), plagioclase index of alteration (PIA) (Fedot et al., 1995), and chemical index of weathering (CIW) (Harnois, 1988). Using the method proposed by McLennan (1993),

TABLE 3 Concentrations of rare elements in clastic rock from the Shihuigou section, North Qilian belt.

Sample	La	Ce	Pr	Nd	Sm	Eu	Gd	Tb	Dy	Ho	Er	Tm	Yb	Lu	ΣREE	δEu	(La/Yb)N	(La/Sm)N	(Gd/Yb)N
SHP-B16	31.10	55.00	6.19	25.30	4.26	1.02	3.76	0.66	3.41	0.81	1.98	0.34	2.15	0.37	136.36	0.78	10.38	4.71	1.45
SHP-B17	34.90	64.00	7.80	27.30	5.42	1.22	4.47	0.83	4.33	0.94	2.31	0.46	2.86	0.42	157.26	0.76	8.75	4.16	1.29
SHP-B18	31.20	55.50	6.62	25.00	4.87	1.18	4.06	0.74	3.62	0.80	2.23	0.39	2.48	0.38	139.07	0.81	9.02	4.14	1.35
SHP-B19	32.90	59.80	7.52	26.70	5.19	1.33	4.20	0.75	3.94	0.90	2.34	0.45	2.54	0.36	148.91	0.87	9.29	4.09	1.37
SHP-B20	35.60	60.20	7.51	27.40	5.43	1.25	4.28	0.76	3.96	0.93	2.21	0.41	2.64	0.38	152.95	0.79	9.67	4.23	1.34
SHP-B21	27.90	62.90	8.05	27.50	5.24	0.93	4.56	0.72	3.98	0.72	1.86	0.45	2.78	0.37	147.95	0.58	7.20	3.44	1.36
SHP-B22	37.50	63.80	7.96	29.30	5.29	1.34	4.58	0.79	4.21	0.88	2.41	0.43	2.87	0.42	161.78	0.83	9.37	4.58	1.32
SHP-B23	32.40	55.90	7.06	26.30	4.71	1.03	4.09	0.68	3.78	0.80	2.09	0.39	2.41	0.36	142.00	0.72	9.64	4.44	1.40
SHP-B24	27.50	52.30	6.21	23.50	4.25	0.88	3.45	0.58	3.12	0.65	1.65	0.35	2.20	0.35	126.99	0.70	8.97	4.18	1.30
SHP-B25	34.50	58.10	7.61	27.70	5.46	1.08	4.34	0.75	3.99	1.02	2.46	0.45	2.88	0.42	150.76	0.68	8.59	4.08	1.25
SHP-B26	31.50	59.60	7.45	29.50	6.17	1.24	4.79	0.94	5.21	1.20	2.94	0.54	3.47	0.53	155.07	0.70	6.51	3.30	1.14
SHP-B27	39.40	73.70	9.09	32.40	7.37	1.32	5.28	0.92	4.52	1.02	2.59	0.47	3.24	0.44	181.76	0.65	8.72	3.45	1.35
SHP-B28	32.80	58.50	7.34	26.80	4.98	1.18	4.34	0.80	4.40	0.99	2.52	0.45	3.13	0.45	148.68	0.78	7.52	4.25	1.15
SHP-B29	26.20	50.20	5.89	23.00	4.84	0.66	3.86	0.74	3.74	0.93	2.35	0.45	3.03	0.44	126.33	0.47	6.20	3.49	1.05
SHP-B30	37.50	69.20	8.39	33.10	6.64	1.29	5.18	0.93	4.82	1.07	2.58	0.52	3.27	0.48	174.97	0.67	8.23	3.65	1.31
SHP-B31	32.40	62.60	7.27	28.70	5.96	1.32	5.05	0.91	5.07	1.21	2.78	0.58	3.73	0.54	158.13	0.74	6.23	3.51	1.12
SHP-B32	36.70	68.00	8.17	28.00	6.32	0.98	4.85	0.86	4.24	0.96	2.64	0.52	3.36	0.52	166.12	0.54	7.83	3.75	1.19
SHP-B33	43.90	80.70	10.30	36.80	7.44	1.21	5.95	0.98	4.75	1.03	2.67	0.48	3.16	0.49	199.85	0.56	9.97	3.81	1.56
SHP-B34	34.40	65.20	7.91	28.90	6.11	0.99	4.56	0.78	3.95	0.89	2.29	0.40	2.66	0.41	159.45	0.57	9.28	3.63	1.42
SHP-B35	46.20	80.00	10.20	37.60	7.27	1.39	5.96	1.04	5.23	1.08	2.85	0.50	3.75	0.50	203.57	0.65	8.84	4.10	1.31

(Continued on the following page)

TABLE 3 (Continued) Concentrations of rare elements in clastic rock from the Shihuigou section, North Qilian belt.

Sample	La	Ce	Pr	Nd	Sm	Eu	Gd	Tb	Dy	Ho	Er	Tm	Yb	Lu	∑REE	δEu	(La/Yb)N	(La/Sm)N	(Gd/Yb)N
SHP-B36	42.40	73.30	8.68	34.30	6.73	1.37	5.53	1.00	4.45	1.10	2.54	0.50	3.19	0.48	185.57	0.69	9.53	4.07	1.43
SHP-B37	38.90	70.60	8.09	34.20	6.22	1.36	5.19	0.85	4.11	0.97	2.35	0.41	2.87	0.42	176.54	0.73	9.72	4.04	1.50
SHP-B38	36.50	64.80	8.41	30.70	6.01	1.04	5.00	0.85	4.47	0.92	2.27	0.42	2.89	0.43	164.71	0.58	9.06	3.92	1.43
SHP-B39	38.00	78.30	8.36	31.80	6.22	1.07	4.71	0.79	4.96	0.86	2.23	0.40	2.65	0.37	180.73	0.60	10.29	3.94	1.47
SHP-B40	37.20	69.00	8.43	30.70	6.16	1.17	8.29	0.85	4.50	1.08	2.54	0.49	3.31	0.44	174.16	0.50	8.06	3.90	2.07
SHP-B61	22.70	45.10	4.98	20.00	4.58	0.85	4.25	0.76	3.92	0.92	2.06	0.43	2.55	0.39	113.48	0.59	6.39	3.20	1.38
SHP-B62	20.90	42.90	4.51	17.00	3.53	0.61	2.92	0.53	2.56	0.61	1.56	0.27	1.70	0.26	99.86	0.58	8.82	3.82	1.42
SHP-B63	15.00	33.60	3.40	13.00	2.43	0.97	2.04	0.36	1.84	0.39	0.98	0.52	1.19	0.18	75.89	1.33	9.04	3.98	1.42
SHP-B64	13.40	29.20	2.93	10.80	2.30	0.52	1.80	0.31	1.47	0.34	0.82	0.16	1.10	0.16	65.32	0.77	8.74	3.76	1.35
SHP-B65	8.58	21.40	1.81	7.18	1.36	0.32	1.23	0.22	1.10	0.30	0.69	0.14	0.90	0.12	45.34	0.74	6.82	4.07	1.13
SHP-B66	32.50	61.70	7.12	25.90	4.85	0.96	3.87	0.64	2.78	0.61	1.72	0.29	1.95	0.31	145.20	0.68	11.95	4.33	1.64
SHP-B67	15.30	31.20	2.67	10.80	1.82	0.34	1.51	0.25	1.15	0.26	0.71	0.13	0.86	0.13	67.13	0.63	12.72	5.43	1.45
SHP-B68	36.30	67.80	6.97	27.00	4.93	0.89	4.20	0.58	3.00	0.63	1.71	0.34	2.25	0.35	156.94	0.60	11.57	4.75	1.54
SHP-B69	11.60	24.00	2.19	9.02	1.48	0.30	1.37	0.23	0.99	0.27	0.67	0.12	0.83	0.13	53.20	0.65	10.00	5.06	1.36
SHP-B70	12.40	24.10	2.37	9.25	1.67	0.35	1.52	0.26	1.26	0.30	0.72	0.13	0.84	0.11	55.29	0.68	10.59	4.79	1.50
PAAS	38.20	79.60	8.83	33.90	5.55	1.08	4.66	0.77	4.68	0.99	2.85	0.41	2.82	0.43	184.77		9.72	4.44	1.37

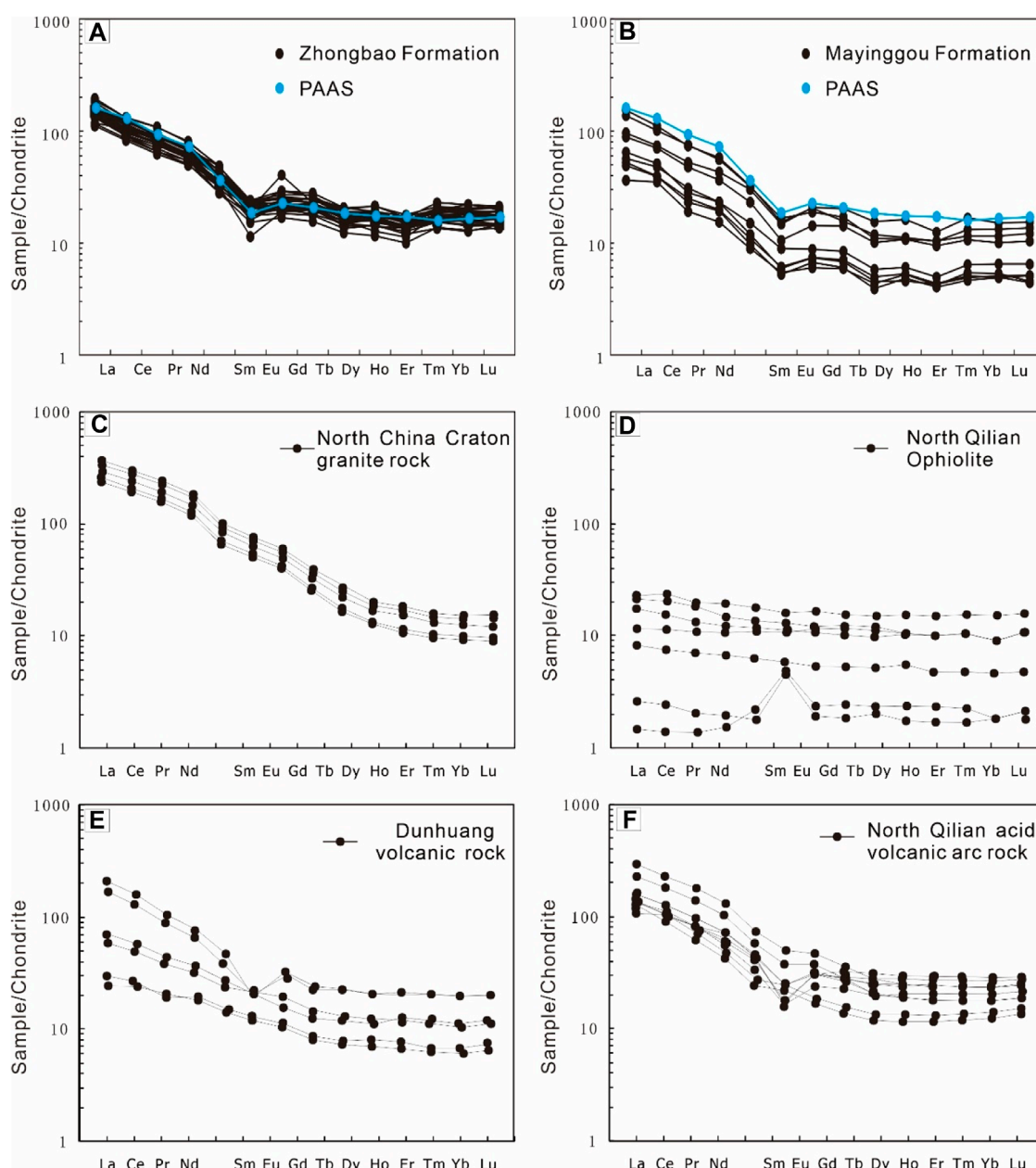


FIGURE 5

(A) Zhongbao Formation Clastic rock REE pattern; (B) Mayinggou Formation Clastic rock REE pattern; (C) North China Craton granite rock REE pattern; (D) North Qilian Ophiolite REE pattern; (E) Dunhuang volcanic rock REE pattern; (F) North Qilian acid volcanic arc rock REE pattern.

the CIA, CIW, and PIA values of Zhongbao–Mayinggou formation samples were calculated, and the results are shown in Table 1.

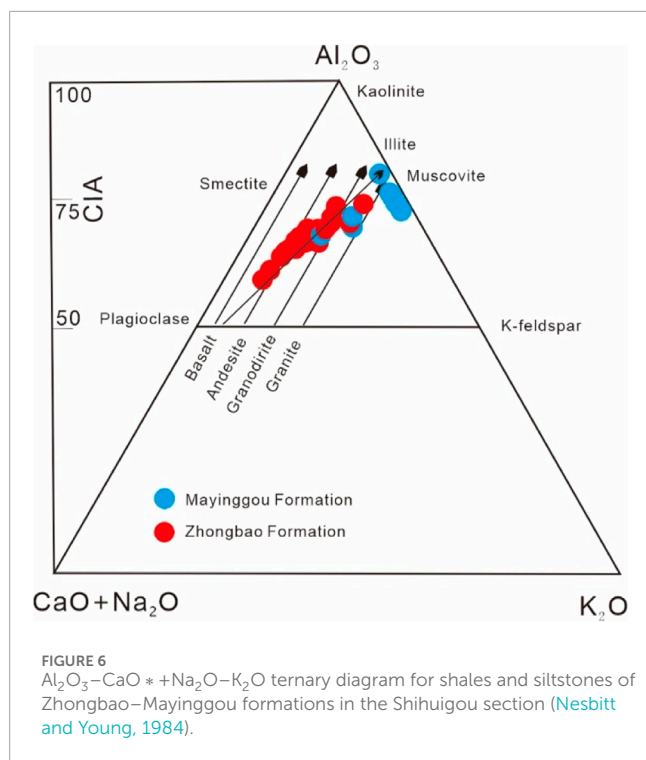
In this paper, the CIA was used to understand the intensity of chemical weathering in the provenance areas. The CIA can use the formula (molecular ratio) to calculate

$$\text{CIA} = 100 \times \left[\frac{\text{Al}_2\text{O}_3}{(\text{Al}_2\text{O}_3 + \text{Na}_2\text{O} + \text{CaO} * + \text{K}_2\text{O})} \right] \quad (\text{Nesbitt and Young, 1982}).$$

In the equation, CaO * is the amount of CaO added to the silicate component of the rock. The CaO content was corrected to be the contribution of carbonate. The ratio of dolomite to calcite is difficult to determine. Therefore, the hypothesis of Bock

et al. (1998) is adopted. It states that CaO values were used only in $\text{CaO} < \text{Na}_2\text{O}$; if $\text{Na}_2\text{O} > \text{CaO}$, CaO is assumed to be Na_2O . Based on the classification method of Fedo et al. (1985), we have included the research results of chemical weathering intensity of some glacial sediments in different regions (Nesbitt and Young, 1982; Nesbitt and Young, 1989; Nesbitt et al., 1996; Chen et al., 2014).

At the Ordovician–Silurian boundary, the CIA value of Zhongbao Formation samples decreased first and then increased; then, there was a greater degree of repetition, from bottom up, ranging from 59.98 to 70.61 (average 65.83). The CIA value of



the lower part of the Zhongbao Formation was between 66.71 and 74.46 (average 70.08), which decreased to the lowest point. The CIA value of the upper part of the Zhongbao Formation increased significantly, ranging from 66.8 to 73.97 (average 70.19). At the top part of the Zhongbao formation, the value decreased to 73.86. Upward, the CIA value quickly recovered to a higher value (81.31) at the bottom part of the Mayinggou Formation. The CIA value of the Mayinggou Formation increased from bottom to top, mainly ranging from 71.26 to 81.31, with an average of 74.49.

The trend of the CIW and PIA values in Zhongbao-Mayinggou formations is similar to the CIA values. The CIW and PIA values of the bottom of the Zhongbao Formation samples range from 61.64 to 78.75 and 64.59 to 98.92, respectively. At the lower part of the Zhongbao Formation, they increase from 72.34 to 87.72 and 75.51 to 90.27, and the upper part is higher. The values at the top of the Zhongbao Formation are 70.77–82.19 and 73.68–84.80. At the bottom part of the Mayinggou Formation, the values of the CIW and PIA rapidly recover to higher values (90.02 and 92.74). The CIW and PIA values of the Mayinggou formation increase from bottom up gradually, which range from 78.75 to 98.02 (average 94.00) and 74.49 to 97.51 (average 92.42), respectively.

Generally speaking, a high CIA value (80–100) directs humid and hot tropical climate environments and strong chemical weathering. A low CIA value (50–60) directs a cold and arid climate and weak chemical weathering. Medium CIA values (60–80) direct humid and warm climate environments and moderate chemical weathering (Fedó et al., 1995; Yan et al., 2010; Ma et al., 2015).

The CIA values of the Lower Zhongbao Formation (59.98–70.61) indicate a low degree of chemical weathering, which may indicate

the arid and cold climatic environments in the source region. All the above are in accordance with the widespread presence of glaciers in the Late Ordovician (Huff et al., 1992; Bergström et al., 1995, 2004; Chen et al., 2006; Melchin and Holmden, 2006; Astini et al., 2007; Yan et al., 2009a, 2009b; Fan et al., 2009; Ge et al., 2019). In the upward direction, the CIA value of the Zhongbao Formation increased from 66.71 to 74.46, and the CIA value of the top of the Zhongbao Formation continued to be low ($CIA_{B40} = 66.80$), varying between 73.83 and 73.97. These values indicate a humid and warm climate and weak weathering of sediments (Nesbitt and Young, 1982, 1989). The CIA values return to relatively high values at the base of the Mayinggou Formation ($CIA_{B61} = 81.31$), which may indicate the beginning of warming and the end of glaciation (Figure 2).

Weathering can also be assessed using CIW and PIA values. The CIW values of the Zhongbao and Mayinggou formations vary from 64.59 to 98.89, which indicate that the source rock weathering degree is moderate to severe ($CIW_{B40} = 70.77$; $CIW_{B61} = 97.52$). Because the method uses total aluminum and does not adjust for aluminum in potassium feldspar, the obtained CIW values are misguided because they produce very high dates for rocks high in potassium content, whether chemically weathered or not, and therefore, they cannot be used directly where the substrate composition changes (Fedó et al., 1995) (Figure 2). The unweathered plagioclase PIA value is 50, and the maximum PIA value is 100 (hydrargillite and kaolinite) (Fedó et al., 1995). The two formation PIA values range from 61.64 to 98.4 ($PIA_{B40} = 73.86$; $PIA_{B61} = 98.03$), showing a moderate-to-high degree of decomposition decay.

Lower Sr/Cu ratios usually indicate a relatively warm and humid paleoclimate, where $Sr/Cu > 10.0$ indicates cold and dry climatic conditions, $5.0 < Sr/Cu < 10.0$ reflects semihumid-semiarid conditions, and $Sr/Cu < 5.0$ indicates warm and humid conditions (Zhang et al., 2023). In this study, $CaO < 7.0\%$ was selected as the threshold to exclude the influence of carbonation on the Sr concentration (Madhavaraju, 2015; Wei and Algeo, 2020).

The paleoclimate characteristics reflected by the Sr/Cu ratios are consistent, and the paleoclimate ranges from cool and arid climatic environments ($3.34 < Sr/Cu < 10.18$) in the Lower Zhongbao Formation to a humid and warm climate ($0.94 < Sr/Cu < 3.51$) in the top of the Zhongbao Formation. The Sr/Cu values return to relatively low values at the base of the Mayinggou Formation ($Sr/Cu_{B62} = 1.07$), which may indicate the beginning of warming and the end of glaciation (Figure 2).

According to the A-CN-K diagram (Nesbitt and Young, 1984) (Figure 6), the two formation samples are located above the plagioclase-potassium feldspar junction, with a good linear trend extending toward end A apex. These study samples were mainly gathered between granite and andesite sources. Due to the occurrence of post-sedimentary potassium metasomatism, the weathering trend line deviated from the predicted line and moved toward the apex of K_2O (Figure 6, dotted arrow line). On the A-CN-K diagram, the sample is plotted at a commensurate position between 50 and 75. On the A-CN-K ternary diagram, the sample is plotted at a commensurate position between 50 and 75 (Fedó et al., 1996). It is inferred that the weathering intensity of the hydrocarbon source area is moderate. All of these infer that the weathering intensity of the source area is moderate.

5.2 Provenance and tectonic setting

The geochemistry of sediments is always influenced by hydraulic sorting, which controls the distribution of some trace elements (Armstrong-Altrin et al., 2014). Sc is concentrated in mafic rocks, while Zr is concentrated in zircon. So, zircon can be traced using the Zr/Sc ratio. Zircon enrichment in clastic sedimentary rocks can be studied in Zr/Sc and Th/Sc relationships (McLennan, 1993). Zr/Sc ratios vary significantly with Th/Sc ratios in mature or recirculated sediments, while Th/Sc is generally positively correlated with Zr/Sc in first-cycle sediments. These depend on the character of the provenance rocks (McLennan, 1993). In the Zr/Sc versus Th/Sc scatter plot (Figure 7), the two formation samples appear along the variation trend of rock magmatic composition on the whole, indicating that no notable sedimentary sorting and recirculation occurred in the rocks.

The geochemical value of the clastic sediments is dominantly used to ascertain the source area and structural setting (Cullers, 1995; McLennan, 1993; Armstrong-Altrin et al., 2004; Armstrong-Altrin et al., 2012; Armstrong-Altrin, 2015; Zaid, 2012; Zaid, 2015; Madhavaraju et al., 2017; Madhavaraju et al., 2019; Madhavaraju et al., 2021). The sandstones from Zhongbao and Mayinggou formations were plotted in the intermediate and felsic field (Figure 8) from the SiO₂ vs. Al₂O₃/TiO₂ diagram (Le Bas et al., 1986).

Girty et al. (1996) argued that if the clastic sedimentary rocks were derived from felsic rocks, the specific values of Al₂O₃ and TiO₂ would be between 19 and 28, and if the clastic sediments were derived from basic rocks, the Al₂O₃/TiO₂ ratio would be less than 14. The Al₂O₃/TiO₂ ratio of the two formations ranged from 16.9 to 47.71, with an average value of 22.76, reflecting that the source rocks were mainly felsic rocks. Furthermore, Roser and Korsch (1988) established a discriminant formula for the source of sediments. It can be observed from the F1–F2 and F3–F4 discriminant maps (Figure 9) that the provenance of the two formation samples is mainly sedimentary rocks.

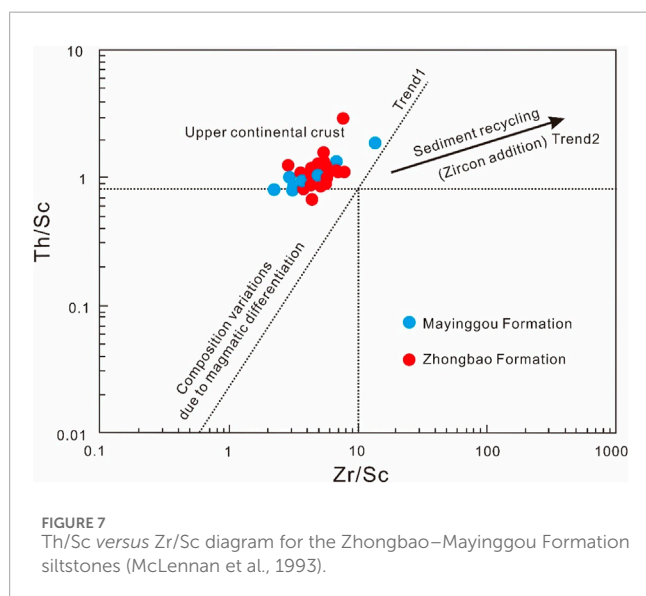


FIGURE 7
Th/Sc versus Zr/Sc diagram for the Zhongbao–Mayinggou Formation siltstones (McLennan et al., 1993).

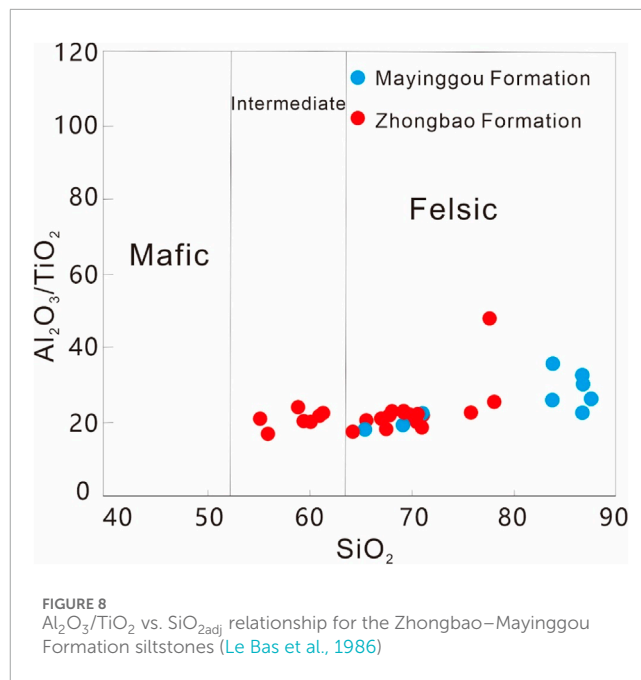
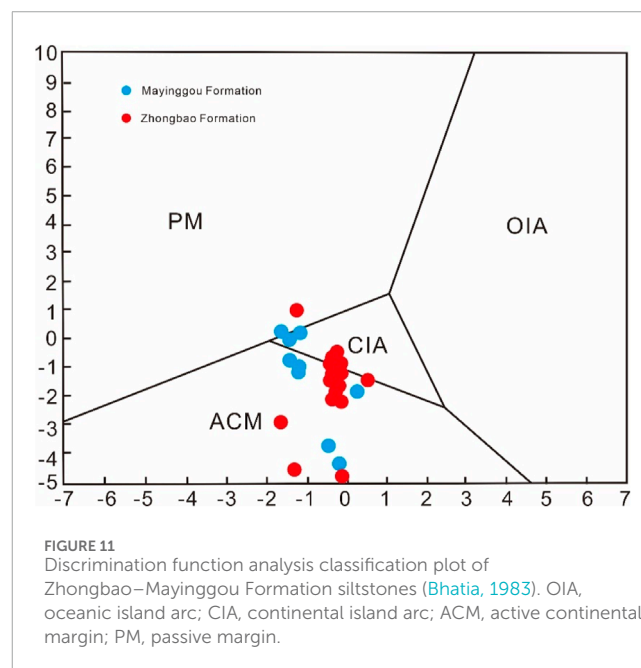
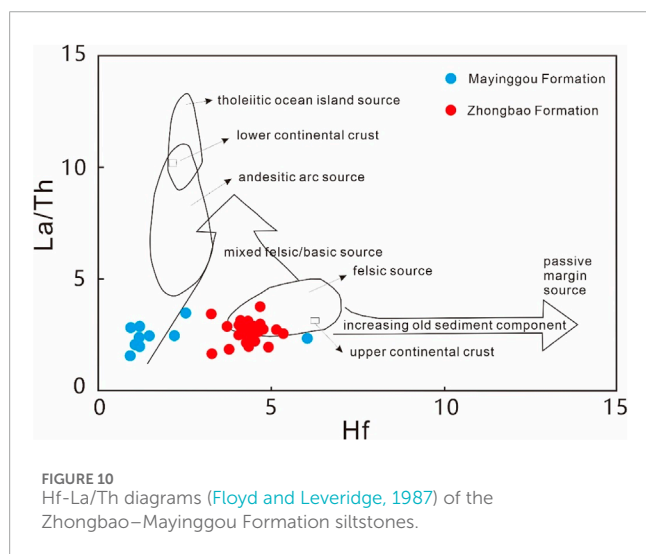
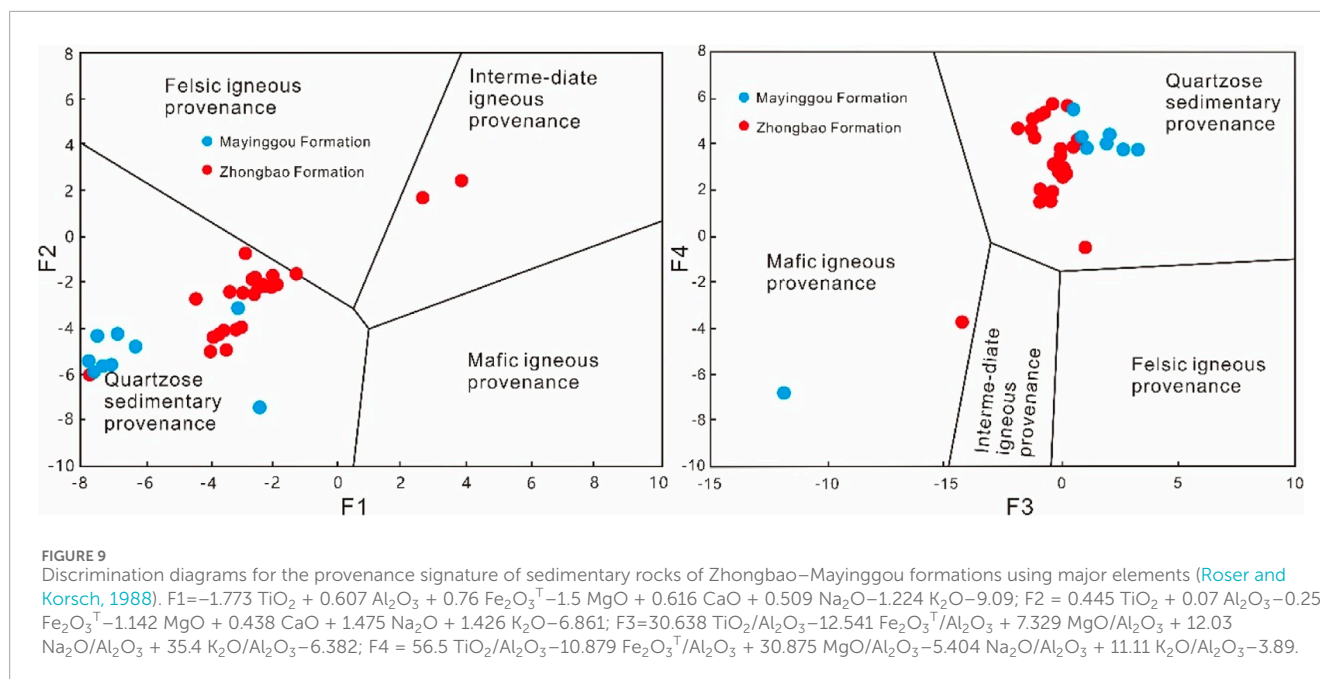


FIGURE 8
Al₂O₃/TiO₂ vs. SiO_{2adj} relationship for the Zhongbao–Mayinggou Formation siltstones (Le Bas et al., 1986)

According to the REE patterns (Figure 5A,B), the LREE section dips show a notable right decrease, showing medium–low fractionation of LREEs, and the HREE section has a smaller slope, indicating weak fractionation of HREEs. The North China Craton granite shows weakly negative Eu anomalies (Eu/Eu* = 0.86–1.13) and enriched LREE patterns with high (La/Yb) ratios (60.5–90.0) in the REE patterns (Figure 5C) (Zhou et al., 2011). The North Qilian ophiolite generally features a weak negative Eu anomaly (Eu/Eu* = 0.77–1.0) and slightly enriched REE pattern ((La/Yb) N = 1.01–2.56) (Figure 5D) (Song et al., 2013). The Dunhuang volcanic rocks display moderate fractionation between LREEs and HREEs ((La/Yb) N = 3.62–4.38), with no Eu anomalies (Eu/Eu* = 0.92–1.05) (Figure 5E) (Wang et al., 2017). The North Qilian volcanic arc rocks generally feature medium–low fractionation of LREEs to HREEs ((La/Yb) N = 6.48–23.28); the LREE section dips steeply, which is shown as a notable right decrease (Figure 5F) (Liang, 2017). A comparison with the different source rocks located near the study area shows that the REE characteristics of the samples from the Zhongbao–Mayinggou formations are in agreement with the North Qilian volcanic arc rocks. These indicate that the formation environment of the Zhongbao–Mayinggou formation sedimentary rocks was mainly related to the active continental margin volcanic arc rocks.

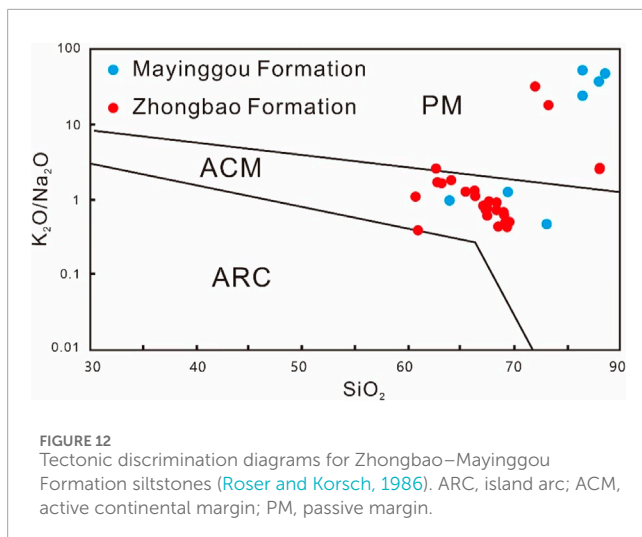
The La/Th–Hf diagram is a widely used source identification map (Gu, et al., 2002; Armstrong-Altrin et al., 2004). Several trace elements, such as Hf, La, and Th, were considered steady during sedimentation, so their concentration and element ratio can be used to distinguish provenance (Taylor and McLennan, 1985; Bhatia and Crook, 1986). The Hf vs. La/Th diagram is widely used to discriminate the source area (Floyd and Leveridge, 1987; Gu, et al., 2002; Armstrong-Altrin et al., 2004). In the Hf–La/Th discrimination graph (Figure 10), most study samples are dispersed in or near long silicon source fields and felsic/basic source-mixed regions.



REEs and Th are enriched in felsic magmatic rocks and their weathering products, while Cr, Sc, and Co are enriched in felsic magmatic rocks (Armstrong-Altrin et al., 2013). The ratios of La/Sc, Cr/Th, Th/Sc, and Th/Co were significantly different in mafic and felsic rocks, which could offer information about the source area (Wronkiewicz and Condie, 1989; Condie and Wronkiewicz, 1990; Armstrong-Altrin et al., 2013). The La/Sc, Th/Co, Cr/Th, and Th/Sc ratios are closer to those of felsic provenances than those of basic source rocks (Table 2), suggesting that clastic sediments are derived from felsic source rocks.

Sedimentary rocks, where rare earth elements are less active and less soluble in water, can also provide important information about the source area (Taylor and McLennan, 1985; Bhatia and Crook, 1986; Floyd and Leveridge, 1987; Gu et al., 2002). The chondrite-normalized rare earth model of the two formation samples is

shown in Figure 5. The distribution pattern of the two formation samples is similar to those of PAAS and upper continental crust normalization values (UCC), indicating that the study samples came from upper crustal rocks. The two formation samples showed negative Eu anomalies compared with UCC and PAAS ($\text{Eu}/\text{Eu}^* = 0.42\text{--}0.81$, $\delta\text{Eu}_{\text{AVG}} = 0.68$). Overall, it can be inferred that the study clastic sediments were perhaps sourced from the felsic rocks. It was probably positioned on thinned continental or transitional continental crust, a situation that resulted in a lack of volcanic material more felsic than andesite (Hou et al., 2018). All of these observations imply that the rocks of the study area may come from the active continental margin background.

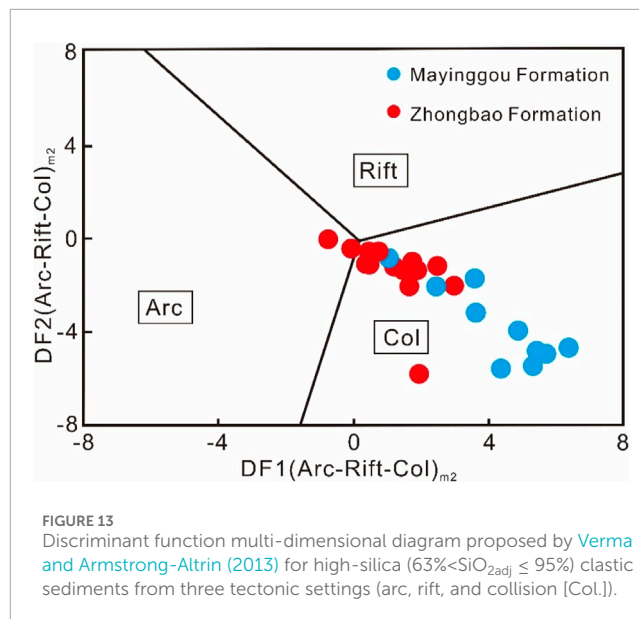


The structural setting of the Zhongbao and Mayinggou formations is a key factor restricting the Paleozoic tectonic history of Northern Qilian and northern Tibetan Plateau. Structural background discriminant graphs based on the major and trace elements are widely used to judge the tectonic setting of the sedimentary basins (Roser and Korsch, 1988; Purevjav and Roser, 2012; Yan et al., 2012; Hou et al., 2020; Hou et al., 2021; Zaid, 2015; 2017a; 2017b; Roser and Korsch, 1986; Roser and Korsch, 1988; Bhatia and Crook, 1986; Purevjav and Roser, 2012; Bhatia, 1983; Bhatia, 1985; Ramirez-Montoya et al., 2021).

The tectonic environment of the unknown basin was evaluated using the detrital principal element diagram introduced by Bhatia (1983) and Roser and Korsch (1986). In the binary discriminant function diagram introduced by Bhatia (1983), two formations of plot samples are observed in the active continental margin field (Figure 11). In the ternary diagrams proposed by Roser and Korsch (1988), the active continental environment was the most probable scenario for the provenance (Figure 12), and few samples fall in the passive margin, affected by metamorphic and tectonic events, so their plotted points were sparsely distributed.

Two new discriminant functions, which were based on the major elements for the structural discrimination of siliceous clastic sedimentary rocks, were proposed by Verma and Armstrong-Altrin (2013). They are used to distinguish the tectonic environments of continental or island arc, collision, and rift. The discrimination graphs can have two scopes, high-silica type (63%–95%) and low-silica type (35%–63%), according to the content of $\text{SiO}_{2\text{adj}}$. The content of SiO_2 in the detrital sediments of the two formations is mostly >63%. The high silicon diagram introduced by Verma and Armstrong-Altrin (2013) was used to confirm the possible tectonic environment of the provenance region. The discriminant graph result provides a conclusion that the study sedimentary rocks came from an active continental margin zone (Figure 13).

Some trace elements with low activity, such as Zr, Y, Th, Sc, and Nb, are most suitable for distinguishing sedimentary

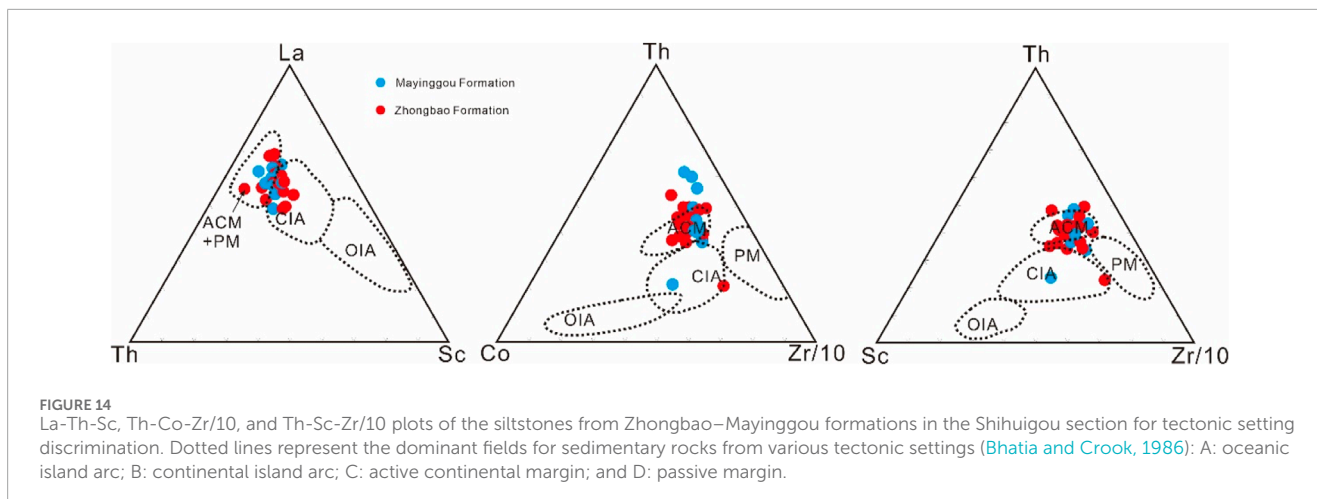


provenance and tectonic environment (Bhatia, 1985; Bhatia and Crook, 1986). In the diagrams of La-Th-Sc, Th-Co-Zr/10, and Th-Sc-Zr/10 introduced by Bhatia and Crook (1986), most of the two formation samples were located in or near the active continental margin field Figure 14. Although there are certain limitations in each provenance discrimination graph, it can be confirmed from each provenance discrimination diagram that the two formations of sandstones mainly come from the active continental margin. In conclusion, the global geochemical features of the discriminant graphs indicate that the tectonic setting of the provenance area is highly possible in the North Qilian active continental margin volcanic arc rocks.

5.3 Sedimentary history of the North Qilian area across the Late Ordovician–Early Silurian

Regional sea level changes are usually controlled by global sea level changes, paleoclimate, sediment supply, and tectonic activity. In the Upper Ordovician, under the influence of the Caledonian movement, the tectonic compression of the North Qilian orogenic belt continued to intensify (Zuo and Liu, 1987; Liu, 1988; Xia et al., 1996; Zuo and Wu, 1997; Xu et al., 2000; Cowgill et al., 2003). Due to the accretion of the North China plate and the Middle Qilian block, the uplift around the North Qilian belt has been expanding, and the interior has been bending downward. The basement of the basin has decreased, but the sea level has risen relatively (Hüs et al., 1995; Yan et al., 2007; Xiao et al., 2009; Yan et al., 2010; Yuan and Yang, 2015). The Late Ordovician was a period of upheaval in the earth system (Xu et al., 1994; Xia et al., 1996; Zhang et al., 1997; Xia et al., 1998; Zhang et al., 1998; Xia et al., 2003; Song et al., 2013).

During the Ordovician–Silurian transition, the North Qilian orogenic belt was influenced by the mass extinction, the end-Ordovician oceanic upturn, the continental shelf environment



surrounded by local plate tectonics and orogenic uplift in the lower paleolatitude, and the fluctuation in the sea level rise (Li et al., 2017a, b; Yuan and Yang, 2015; Xiao et al., 2009). The Shihuigou outcrop area developed into a semi-closed basin constrained by marginal uplift and deposited silty mudstone in the lower part of the Zhongbao Formation. Then, the Gondwana glaciation started, the climate began to dry and cool, ice continued to form, and the global sea level dropped (Fan et al., 2009; Rong et al., 2010), which stayed the same with the decrease in CIA values in the lower Zhongbao Formation (from 74.49 to 66.71). Black chert was deposited in the Yongdeng area of the upper Zhongbao Formation because the rate of basement decrease was greater than the rate of sea level decline caused by glaciation. In the Early Silurian, the collision between the Center Qilian block and the North China plate intensified, the global sea levels rose, the glaciation ended, and the climate began to get wetter and warmer (Zhang et al., 2000; Yan et al., 2009a), which stayed the same with the increase in the CIA value (from 73.86 to 81.31) at the bottom of the Mayinggou Formation. Ice melting and basin basement decrease promoted the deposition of silty mudstone at the bottom of Mayinggou formation.

6 Conclusion

On account of the petrological characteristics and geochemical analysis of Zhongbao–Mayinggou formation (Late Ordovician–Early Silurian) siltstones in Shihuigou outcrop, the following conclusions are drawn:

- (1) The studied clastic sedimentary rocks consist mainly of clay mineral, quartz, and few mica. Geochemically, the samples from the Zhongbao–Mayinggou formations have chondrite-normalized REE patterns similar to that of the North Qilian volcanic arc rocks, which are characterized by weak negative Eu anomaly, with a slight LREE enrichment accompanied by a flat HREE trend.
- (2) The CIA, CIW, and PIA indexes showed that the weathering environment in the study area changed from weak to moderate

to intense. The undulation of the CIA value reflects the change in climate from cold to warm in the Ordovician to the Silurian. The CIA value of the upper part of the Zhongbao Formation was continuously low (66.71%–73.97%), and the climate was relatively dry and cold, which was the same with the wide range of Gondwana glaciation in these periods. The CIA values return to a relatively high value (81.31%) at the base of the Mayinggou Formation, which may indicate the beginning of warming and the end of glaciation.

- (3) The $Al_2O_3-(CaO * +Na_2O)-K_2O$ triangular plots, Hf-La/Th, and $SiO_2-Al_2O_3/TiO_2$ bivariate plots infer that the source of the siltstones in the two formations is mostly from the felsic igneous rocks. The major element plot graphs and Th-Sc-Zr/10, La-Th-Sc, and Th-Co-Zr/10 triangulation reflect that the clasts of the Zhongbao–Mayinggou formations come from the active continental margin.
- (4) Across the Late Ordovician–Early Silurian, the end of the Ordovician glaciation and the tectonic activity dominantly controlled the deposition of black chert and silty mudstone in the Zhongbao–Mayinggou formations in the Shihuigou section, North Qilian belt.

Data availability statement

The original contributions presented in the study are included in the article/Supplementary Material; further inquiries can be directed to the corresponding author.

Author contributions

YX: writing–original draft and writing–review and editing. QH: writing–original draft and writing–review and editing. CM: writing–review and editing.

Funding

The author(s) declare that financial support was received for the research, authorship, and/or publication of this article. This study was financially supported by the Liubaojun Academician Foundation of Chengdu Center of China Geological Survey (characteristics of source rocks in Datangpo formation, Sichuan Basin) and the China Geological Survey Project (No. DD20230266).

Acknowledgments

The authors thank the journal reviewers for their very helpful and constructive comments, which helped improve the manuscript.

References

- Akarish, A. I., and El-Gohary, A. M. (2008). Petrography and geochemistry of lower Paleozoic sandstones, East Sinai, Egypt: implications for provenance and tectonic setting. *J. Afr. Earth Sc.* 52 (1–2), 43–54. doi:10.1016/j.jafrearsci.2008.04.002
- Algeo, T. J., Marengo, P. J., and Saltzman, M. R. (2016). Co-evolution of oceans, climate, and the biosphere during the ‘Ordovician Revolution’: a review. *Palaeogeogr. Palaeoclimatol. Palaeoecol.* 458, 1–11. doi:10.1016/j.palaeo.2016.05.015
- Armstrong-Altrin, J. S. (2015). Evaluation of two multidimensional discrimination diagrams from beach and deep-sea sediments from the Gulf of Mexico and their application to Precambrian clastic sedimentary rocks. *Int. Geol. Rev.* 57, 1446–1461. doi:10.1080/00206814.2014.936055
- Armstrong-Altrin, J. S., Lee, Y. I., Kasper-Zubillaga, J. J., Carranza-Edwards, A., Garcia, D., Eby, N., et al. (2012). Geochemistry of beach sands along the western Gulf of Mexico, Mexico: implication for provenance. *Chem. Erde. Geochem.* 72, 345–362. doi:10.1016/j.chemer.2012.07.003
- Armstrong-Altrin, J. S., Lee, Y. I., Verma, S. P., and Ramasamy, S. (2004). Geochemistry of sandstones from the Upper Miocene Kudankulam Formation, southern India: implications for provenance, weathering, and tectonic setting. *J. Sediment. Res.* 74, 285–297. doi:10.1306/082803740285
- Armstrong-Altrin, J. S., Nagarajan, R., Lee, Y. I., Kasper-Zubillaga, J. J., and Córdoba-Saldaña, L. P. (2014). Geochemistry of sands along the San Nicolás and San Carlos beaches, Gulf of California, Mexico: implications for provenance and tectonic setting. *Turk J. Earth Sci.* 23, 533–558. doi:10.3906/yer-1309-21
- Armstrong-Altrin, J. S., Nagarajan, R., Madhavaraju, J., Rosalez-Hoz, L., Lee, Y. I., Balam, V., et al. (2013). Geochemistry of the Jurassic and upper Cretaceous shales from the Molango region, Hidalgo, eastern Mexico: implications for source-area weathering, provenance, and tectonic setting. *Comptes Rendus Geosci.* 345, 185–202. doi:10.1016/j.crte.2013.03.004
- Astini, R. A., Collo, G., and Martina, F. (2007). Ordovician K-bentonites in the upper-plate active margin of western Gondwana, (Famatinian ranges): stratigraphic and palaeogeographic significance. *Gondwana Res.* 11, 311–325. doi:10.1016/j.gr.2006.05.005
- Bai, J., Wang, H. L., Zhu, X. H., and Xie, C. R. (2016). Characteristics of olistostromes from the Ordovician Zhongbao Group in Shihuigou area, North Qilian orogenic belt and their palaeogeographic implications. *Geol. China* 43, 977–986.
- Bergström, S. M., Huff, W. D., Kolata, D. R., and Bauert, H. B. (1995). Nomenclature, stratigraphy, chemical fingerprinting, and areal distribution of some Middle Ordovician K-bentonites in Baltoscandia. *GFF* 117, 1–13. doi:10.1080/11035899509546191
- Bergström, S. M., Huff, W. D., Saltzman, M. R., Kolata, D. R., and Leslie, S. A. (2004). The greatest volcanic ash falls in the Phanerozoic: trans-atlantic relations of the Ordovician millbrig and kinnekulle K-bentonites. *Sediment. Rec.* 2, 4–8. doi:10.2110/sedred.2004.4.4
- Bhatia, M. R. (1983). Plate tectonics and geochemical composition of sandstones. *J. Geol.* 91, 611–627. doi:10.1086/628815
- Bhatia, M. R. (1985). Composition and classification of Paleozoic flysch mudrocks of eastern Australia: implications for provenance and tectonic setting interpretation. *Sediment. Geol.* 41, 249–268. doi:10.1016/0037-0738(84)90065-4
- Bhatia, M. R., and Crook, K. A. W. (1986). Trace element characteristics of graywackes and tectonic setting discrimination of sedimentary basins. *Contrib. Mineral. Petrol.* 92 (2), 181–193. doi:10.1007/bf00375292
- Chen, X., Rong, J. Y., Fan, J. X., Zhan, R. B., Mitchell, C. E., Harper, D. A. T., et al. (2006). The global boundary stratotype section and point (GSSP) for the base of the Hirnantian stage (the uppermost of the Ordovician system). *Episodes* 29, 183–196. doi:10.18814/epiugs/2006/v29i3/004
- Chen, X., Rong, J. Y., Li, Y., and Boucot, A. J. (2004). Facies patterns and geography of the Yangtze region, south China, through the Ordovician and Silurian transition. *Palaeogeogr. Palaeoclimatol. Palaeoecol.* 204, 353–372. doi:10.1016/s0031-0182(03)00736-3
- Chen, Y. J., Pei, X. Z., Li, R. B., and Li, Z. V. (2014). Geochemical characteristics and tectonic significance of meta-sedimentary rocks from the Najital Group, eastern section of East Kunlun. *Geoscience* 28 (3), 489–500.
- Condie, K. C., and Wronkiewicz, D. J. (1990). The Cr/Th ratio in Precambrian pelites from the Kaapvaal craton as an index of craton evolution. *Earth Planet. Sci. Lett.* 97, 256–267. doi:10.1016/0012-821x(90)90046-z
- Cowgill, E., Yin, A., Harrison, T. M., and Wang, X. F. (2003). Reconstruction of the Altyn Tagh fault based on U-Pb geochronology: role of back thrusts, mantle sutures, and heterogeneous crustal strength in forming the Tibetan Plateau. *J. Geophys. Res.* 108, 2346. doi:10.1029/2002jb002080
- Cullers, R. L. (1995). The controls on the major- and trace-element evolution of shales, siltstones and sandstones of Ordovician to tertiary age in the Wet Mountains region, Colorado, U.S.A. *U.S.A. Chem. Geol.* 123, 107–131. doi:10.1016/0009-2541(95)00050-v
- Cullers, R. L., and Podkovyrov, V. N. (2000). Geochemistry of the Mesoproterozoic Lakhanda shales in southeastern Yakutia, Russia: implications for mineralogical and provenance control, and recycling. *Precambrian Res.* 104, 77–93. doi:10.1016/s0301-9268(00)00090-5
- Dong, Y. P., and Santosh, M. (2016). Tectonic architecture and multiple orogeny of the Qinling Orogenic Belt, central China. *Gondwana Res.* 29, 1–40. doi:10.1016/j.gr.2015.06.009
- Du, Y. S., Zhu, J., and Gu, S. Z. (2006). Sedimentary geochemistry of cherts from the middle-upper Ordovician in Shihuigou area, North Qilian Orogenic belt and its tectonic implications. *Geol. Rev.* 52, 184–189. [In Chinese with English abstract].
- Fan, J. X., Peng, P. A., and Melchin, M. J. (2009). Carbon isotopes and event stratigraphy near the Ordovician-Silurian boundary, Yichang, South China. *Palaeogeogr. Palaeoclimatol. Palaeoecol.* 276, 160–169. doi:10.1016/j.palaeo.2009.03.007
- Fedo, C. M., Eriksson, K. A., and Krogstad, E. J. (1996). Geochemistry of shales from the Archean (~3.0 Ga) Buhwa Greenstone Belt, Zimbabwe: Implications for provenance and source-area weathering. *Geochim. Cosmochim. Acta.* 60, 1751–1763. doi:10.1016/0016-7037(96)00058-0
- Fedo, C. M., Nesbitt, H. W., and Young, G. M. (1995). Unraveling the effects of potassium metasomatism in sedimentary rocks and paleosols, with implications for paleoweathering conditions and provenance. *Geology* 23, 921–924. doi:10.1130/0091-7613(1995)023<0921:uteopm>2.3.co;2
- Feng, Q. L. (1992). A preliminary study on the radiolarian palaeoecology. *Geol. Sci. Technol. Inf.* 11, 41–46. [In Chinese with English abstract].
- Floyd, P. A., and Leveridge, B. E. (1987). Tectonic environment of the Devonian Gramscatho basin, south Cornwall: framework mode and geochemical evidence from turbiditic sandstones. *J. Geol. Soc. Lond.* 144, 531–542. doi:10.1144/gsjgs.144.4.0531

Conflict of interest

The authors declare that the research was conducted in the absence of any commercial or financial relationships that could be construed as a potential conflict of interest.

Publisher's note

All claims expressed in this article are solely those of the authors and do not necessarily represent those of their affiliated organizations, or those of the publisher, the editors, and the reviewers. Any product that may be evaluated in this article, or claim that may be made by its manufacturer, is not guaranteed or endorsed by the publisher.

- Ge, X. Y., Mou, C. L., Wang, C. S., Men, X., Chen, C., and Hou, Q. (2019). Mineralogical and geochemical characteristics of K-bentonites from the Late Ordovician to the Early Silurian in South China and their geological significance. *Geol. J.* 54, 514–528. doi:10.1002/gj.3201
- Ghienne, J. F. (2003). Late Ordovician sedimentary environments, glacial cycles, and postglacial transgression in the Taoudeni Basin, West Africa. *Palaeogeogr. Palaeoclimatol. Palaeoecol.* 189, 117–145. doi:10.1016/s0031-0182(02)00635-1
- Girty, G. H., Ridge, D. L., and Knaack, C. (1996). Provenance and depositional setting of Paleozoic chert and argillite, Sierra Nevada, California. *J. Sediment. Researc* 66 (1), 107–118. doi:10.1306/d42682ca-2b26-11d7-8648000102c1865d
- Gu, X. X., Liu, J. M., Zheng, M. H., Tang, J. X., and Qi, L. (2002). Provenance and Tectonic Setting of the Proterozoic Turbidites in Hunan, South China: Geochemical Evidence. *J. Sediment. Res.* 72 (3), 393–407. doi:10.1306/081601720393
- Harnois, L. (1988). The CIW index: a new chemical index of weathering. *Sediment. Geol.* 55, 319–322. doi:10.1016/0037-0738(88)90137-6
- Hou, Q., Mou, C. L., Han, Z. Z., Ge, X. Y., and Wang, Q. Y. (2021). Origin of chert in the Upper Ordovician–Lower Silurian: implications for the sedimentary environment of North Qilian Orogen. *Earth Environ. Sci. Trans. R. Soc. Edinb.* 112 (1), 13–28. doi:10.1017/s1755691021000025
- Hou, Q., Mou, C. L., Han, Z. Z., Wang, Q. Y., Tan, Z. Y., and Ge, X. (2020). Petrography and geochemistry of the Lower Silurian sandstones from the Angzangou Formation in the North Qilian Belt, China: implications for provenance, weathering and tectonic setting. *Geol. Mag.* 157, 477–496. doi:10.1017/s0016756819000931
- Hou, Q., Mou, C. L., Wang, Q. Y., and Tan, Z. Y. (2018a). Provenance and tectonic setting of the Early and Middle Devonian Xueshan Formation, the North Qilian Belt, China. *Geol. J.* 53, 1404–1422. doi:10.1002/gj.2963
- Hou, Q., Mou, C. L., Wang, Q. Y., Tan, Z. Y., Ge, X. Y., and Wang, X. P. (2018b). Geochemistry of Sandstones from the Silurian Hanxia Formation, North Qilian Belt, China: Implication for Provenance, Weathering and Tectonic Setting. *Geochem. Int.* 56, 362–377. doi:10.1134/s0016702918040092
- Huff, W. D., Bergström, S. M., and Kolata, D. R. (1992). Gigantic Ordovician volcanic ash fall in North America and Europe: biological, tectonomagmatic, and event-stratigraphic significance. *Geology* 20, 875–878. doi:10.1130/0091-7613(1992)020<0875:govafi>2.3.co;2
- Hüs, K. J., Pan, G., and Sengor, A. M. (1995). Tectonic evolution of the Tibetan Plateau: A working hypothesis based on the archipelago model of orogenesis. *Int. Geol. Rev.* 37, 473–508. doi:10.1080/00206819509465414
- Kato, Y., Nakao, K., and Isozaki, Y. (2002). Geochemistry of Late Permian to Early Triassic pelagic cherts from southwest Japan: implications for an oceanic redox change. *Chem. Geol.* 182, 15–34. doi:10.1016/s0009-2541(01)00273-x
- Ketris, M. P., and Yudovich, Y. E. (2009). Estimations of clarkes for carbonaceous biolithes: world averages for trace element contents in black shales and coals. *Int. J. Coal. Geol.* 78 (2), 135–148. doi:10.1016/j.coal.2009.01.002
- Le-Bas, M. J., Le-Maitre, R. W., Streckeisen, A., and Zanettin, B. (1986). A chemical classification of volcanic rocks based on the total alkali-silica diagram. *J. Petrol.* 27, 745–750. doi:10.1093/petrology/27.3.745
- Lei, Z. H., Dashtgard, S. E., Wang, J., Li, M., Feng, Q. L., Yu, Q., et al. (2019). Origin of chert in Lower Silurian Longmaxi Formation: implications for tectonic evolution of Yangtze Block, South China. *Palaeogeogr. Palaeoclimatol. Palaeoecol.* 529, 53–66. doi:10.1016/j.palaeo.2019.05.017
- Li, S. Z., Jahn, B. M., Zhao, S. J., Dai, L. M., Li, X. Y., Suo, Y. H., et al. (2017a). Triassic southeastward subduction of North China Block to South China Block: insights from new geological, geophysical and geochemical data. *Earth-Science Rev.* 166, 270–285. doi:10.1016/j.earscirev.2017.01.009
- Li, Y., Zhang, T., Ellis, G. S., and Shao, D. (2017b). Depositional environment and organic matter accumulation of Upper Ordovician–Lower Silurian marine shale in the Upper Yangtze Platform, South China. *Palaeogeogr. Palaeoclimatol. Palaeoecol.* 466, 252–264. doi:10.1016/j.palaeo.2016.11.037
- Liang, Z. Y. (2017). *Geological characteristics and tectonic significance of Early Paleozoic Island arc volcanic rocks*. Doctoral Dissertation. Beijing: China University of Geosciences.
- Liu, Z. Q. (1988). *Geological map of the Qinghai-Xizang (Tibetan) plateau and adjacent areas*, 1. Beijing: Geological Publishing House. scale, 1:500000.
- Ma, P. F., Wang, L. C., Wang, C. S., Wu, X. H., and Wei, Y. S. (2015). Organic-matter accumulation of the lacustrine lunpola oil shale, central Tibetan plateau: controlled by the paleoclimate, provenance, and drainage system. *Int. J. Coal. Geol.* 147–148, 58–70. doi:10.1016/j.coal.2015.06.011
- Madhavaraju, J. (2015). *Geochemistry of campanian-maastrichtian sedimentary rocks in the cauvery basin, south India: constrains on paleoweathering, provenance and end cretaceous environments. Chemostratigraphy: concepts, techniques and applications*. Editor M. Ramkumar (Elsevier Special), Volume, 185–214.
- Madhavaraju, J., Armstrong-Altrin, J. S., Pillai, R. B., and Pi-Puig, T. (2021). Geochemistry of sands from the Huatatabampo and Altata beaches, Gulf of California, Mexico. *Geol. J.* 56, 2398–2417. doi:10.1002/gj.3864
- Madhavaraju, J., Pacheco-Olivas, S. A., Gonzalez-Leon, C. M., Espinoza-Maldonado, I. G., Sanchez-Medrano, P. A., Villanueva-Amadoz, U., et al. (2017). Mineralogy and geochemistry of the Lower Cretaceous siliciclastic rocks of the Morita Formation, Sierra San José section, Sonora, Mexico. *J. S. Am. Earth Sci.* 76, 397–411. doi:10.1016/j.jsames.2017.04.001
- Madhavaraju, J., Saucedo-Samaniego, J. C., Löser, H., Espinoza-Maldonado, I. C., Solari, L., Monreal, R., et al. (2019). Detrital zircon record of Mesozoic volcanic arcs in the Lower Cretaceous Mural Limestone, northwestern Mexico. *Geol. J.* 54, 2621–2645. doi:10.1002/gj.3315
- McLennan, S. M. (1993). Weathering and global denudation. *J. Geol.* 101, 295–303. doi:10.1086/648222
- Melchin, M. J., and Holmden, C. (2006). Carbon isotope chemostratigraphy in Arctic Canada: sea-level forcing of carbonate platform weathering and implications for Hirnantian global correlation. *Palaeogeogr. Palaeoclimatol. Palaeoecol.* 234, 186–200. doi:10.1016/j.palaeo.2005.10.009
- Melchin, M. J., Mitchell, C. E., Holmden, C., and Štorch, P. (2013). Environmental changes in the Late Ordovician–early Silurian: Review and new insights from black shales and nitrogen isotopes. *Bulletin* 125 (11–12), 1635–1670. doi:10.1130/b30812.1
- Men, X., Mou, C. L., and Ge, X. Y. (2022). Changes in palaeoclimate and palaeoenvironment in the Upper Yangtze area (South China) during the Ordovician–Silurian transition. *Sci. Rep.* 12 (1), 13186. doi:10.1038/s41598-022-17105-2
- Moosavirad, S. M., Janardhana, M. R., Sethumadhav, M. S., Moghadam, M. R., and Shankara, M. (2011). Geochemistry of lower Jurassic shales of the Shemshak Formation, Kerman Province, Central Iran: provenance, source weathering and tectonic setting. *Chem. Erde. Geochem.* 71, 279–288. doi:10.1016/j.chemer.2010.10.001
- Mou, C. L., Hou, Q., Zheng, B. S., Ge, X. Y., and Zan, B. W. (2020). Sedimentary facies and palaeogeography of the Northern Qilian orogenic during the Silurian. *Sediment. Geol. Tethyan Geol.* 40 (3), 48–58. (in Chinese with English abstract).
- Nesbitt, H. W., and Young, G. M. (1982). Early Proterozoic climates and plate motions inferred from major element chemistry of lutites. *Nature* 299, 715–717. doi:10.1038/299715a0
- Nesbitt, H. W., and Young, G. M. (1984). Prediction of some weathering trends of plutonic and volcanic rocks based on thermodynamic and kinetic considerations. *Geochim. Cosmochim. Acta.* 48, 1523–1534. doi:10.1016/0016-7037(84)90408-3
- Nesbitt, H. W., and Young, G. M. (1989). Formation and diagenesis of weathering profiles. *J. Geol.* 97, 129–147. doi:10.1086/629290
- Nesbitt, H. W., Young, G. M., McLennan, S. M., and Keays, R. R. (1996). Effects of chemical weathering and sorting on the petrogenesis of siliciclastic sediments, with implications for provenance studies. *J. Geol.* 104 (5), 525–542. doi:10.1086/629850
- Paris, F., Elaouad-Debbaj, Z., Jaglin, J. C., Massa, D., and Oulebsir, L. (1995). “Chitinozoans and Late Ordovician glacial events on Gondwana,” in *Ordovician odyssey: short papers for the seventh international symposium on the ordovician system. The Pacific section society for sedimentary Geology*. Editors J. D. Cooper, M. L. Droser, and S. C. Finney (California: Fullerton), 171–176.
- Purevjav, N., and Roser, B. (2012). Geochemistry of Devonian–Carboniferous clastic Sediments of the Tsetserleg terrane, Hangay Basin, central Mongolia: provenance, source weathering, and tectonic setting. *Isl. Arc.* 21, 270–287. doi:10.1111/j.1440-1738.2012.00821.x
- Ramirez-Montoya, E., Madhavaraju, J., and Monreal, R. (2021). Geochemistry of the sedimentary rocks from the Antimonio and Rio Asuncion Formations, Sonora, Mexico: Implications for weathering, provenance and chemostratigraphy. *J. S. Am. Earth Sci.* 106, 103035. doi:10.1016/j.jsames.2020.103035
- Ran, B., Liu, S., Jansa, L., Sun, W., Yang, D., Ye, Y., et al. (2015). Origin of the Upper Ordovician–Lower Silurian cherts of the Yangtze block, South China, and their palaeogeographic significance. *J. Asian Earth Sci.* 108, 1–17. doi:10.1016/j.jseae.2015.04.007
- Rollinson, H. (1993). *Using geochemical data: evaluation, presentation, interpretation*. London: Longman, 1–352.
- Rong, J. Y., and Chen, X. (1987). Faunal differentiation, Biofacies and Lithofacies Pattern of Late Ordovician (Ashgillian) in South China. *Acta. palaeontol. Sin.* 26, 507–545. (in Chinese with English abstract).
- Rong, J. Y., Zhan, R. B., Xu, H. G., Huang, B., and Yu, G. H. (2010). Expansion of the Cathaysian Oldland through the Ordovician–Silurian transition: Emerging evidence and possible dynamics. *Sci. China. Earth. Sci.* 53, 1–17. doi:10.1007/s11430-010-0005-3
- Roser, B. P., and Korsch, R. J. (1986). Determination of tectonic setting of sandstone-mudstone suites using SiO₂ content and K₂O/Na₂O ratio. *J. Geol.* 94, 635–650. doi:10.1086/629071
- Roser, B. P., and Korsch, R. J. (1988). Provenance signatures of sandstone–mudstone suites determined using discriminant function analysis of major-element data. *Chem. Geol.* 67, 119–139. doi:10.1016/0009-2541(88)90010-1
- Song, S. G., Niu, Y., Zhang, L. F., Wei, C., Liou, J. G., and Su, L. (2009). Tectonic evolution of early Paleozoic HP metamorphic rocks in the North

- Qilian Mountains, NW China: new perspectives. *J. Asian Earth Sci.* 35, 334–353. doi:10.1016/j.jseas.2008.11.005
- Song, S. G., Niu, Y. L., Su, L., and Xia, X. H. (2013). Tectonics of the North Qilian orogen, NW China. *Gondwana Res.* 23, 1378–1401. doi:10.1016/j.gr.2012.02.004
- Taylor, S. R., and McLennan, S. M. (1985). *The continental crust: its composition and evolution*. Oxford, UK: Blackwell, 1–311.
- Verma, S. P., and Armstrong-Altrin, J. S. (2013). New multi-dimensional diagrams for tectonic discrimination of siliciclastic sediments and their application to Precambrian basins. *Chem. Geol.* 355, 117–133. doi:10.1016/j.chemgeo.2013.07.014
- Wang, Z. M., Han, C. M., Xiao, W. J., and Sakyi, P. A. (2017). Paleozoic subduction-related magmatism in the Duobagou area, Dunhuang block: constrained by zircon U–Pb geochronology and Lu–Hf isotopes and whole-rock geochemistry of metaigneous rocks. *Lithosphere* 9, 1012–1032. doi:10.1130/1688.1
- Wei, W., and Algeo, T. J. (2020). Elemental proxies for paleosalinity analysis of ancient shales and mudrocks. *Geochimica Cosmochimica Acta* 287, 341–366. doi:10.1016/j.gca.2019.06.034
- Wronkiewicz, D. J., and Condie, K. C. (1989). Geochemistry and provenance of sediments from the Pongola Supergroup, South Africa: Evidence for a 3.0Ga-old continental craton. *Geochimica Cosmochimica Acta* 53, 1537–1549. doi:10.1016/0016-7037(89)90236-6
- Xia, L. Q., Xia, Z. C., and Xu, X. Y. (1996). *Origin of marine volcanic rocks in north Qilian mountains*. Beijing: Geological Publishing House, 1–153. [In Chinese].
- Xia, L. Q., Xia, Z. C., and Xu, X. Y. (1998). Early Paleozoic mid-ocean ridge – ocean island and back-arc basin volcanism in the north Qilian mountains. *Acta Geol. Sin.* 72, 301–312. (In Chinese with English abstract).
- Xia, L. Q., Xia, Z. C., and Xu, X. Y. (2003). Magmagenesis in the Ordovician backarc basins of the Northern Qilian Mountains, China. *Geol. Soc. Am. Bull.* 115, 1510–1522. doi:10.1130/b25269.1
- Xiao, W. J., Brian, F. W., Yong, Y., Yan, Z., Yuan, C., Liu, C., et al. (2009). Early Paleozoic to Devonian multiple-accretionary model for the Qilian Shan, NW China. *J. Asian Earth Sci.* 35 (3–4), 323–333. doi:10.1016/j.jseas.2008.10.001
- Xu, X. Y., Zhao, J. T., Xia, L. Q., and Xia, Z. C. (2003). Tectonic setting implications of rare earth elements in early Paleozoic chert from the Northern Qilian Mountains. *Geol. Rev.* 49, 605–609. [In Chinese with English abstract].
- Xu, Z., Xu, H. F., Zhang, J., Li, H., Zhu, Z., Qu, J., et al. (1994). The Zhoulanshan Caledonian subduction complex in the northern Qilian Mountains and its dynamics (in Chinese). *Acta Geol. Sin.* 68, 1–15.
- Xu, Z. Q., Zhang, J. X., and Li, H. B. (2000). Architecture and orogeny of the northern Qilian orogenic belt, northwestern China. *Geol. Soc. China J.* 43, 125–141.
- Yan, D. T., Chen, D. Z., Wang, Q. C., and Wang, J. G. (2009a). Geochemical changes across the Ordovician–Silurian transition on the Yangtze Platform, South China. *Sci. China. Earth. Sci.* 52, 38–54. doi:10.1007/s11430-008-0143-z
- Yan, D. T., Chen, D. Z., Wang, Q. C., and Wang, J. G. (2010). Large-scale climatic fluctuations in the latest Ordovician on the Yangtze block, South China. *Geology* 38, 599–602. doi:10.1130/g30961.1
- Yan, D. T., Chen, D. Z., Wang, Q. C., Wang, J. G., and Wang, Z. Z. (2009b). Carbon and sulfur isotopic anomalies across the Ordovician–Silurian boundary on the Yangtze Platform, South China. *Palaeogeogr. Palaeoclimatol. Palaeoecol.* 274, 32–39. doi:10.1016/j.palaeo.2008.12.016
- Yan, Z., Wang, Z., Yan, Q., Wang, T., and Guo, X. (2012). Geochemical constraints on the provenance and depositional setting of the Devonian Liuling Group, East Qinling mountains, central China: implications for the tectonic evolution of the Qinling Orogenic Belt. *J. Sediment. Res.* 82, 9–20. doi:10.2110/jsr.2012.4
- Yan, Z., Xiao, W. J., Liu, C. Z., Yuan, C., Li, J. L., et al. (2007). Detrital composition of the Laojunshan Conglomerate and tectonic settings of its source rocks in the Qilian Mountains. *Geol. Bull. China* 25, 83–98.
- Yuan, W., and Yang, Z. Y. (2015). Late Devonian closure of the North Qilian Ocean: evidence from detrital zircon U–Pb geochronology and Hf isotopes in the eastern North Qilian Orogenic Belt. *Geol. Rev.* 1, 182–198. doi:10.1080/00206814.2014.999357
- Zaid, S. M. (2012). Provenance, diagenesis, tectonic setting and geochemistry of Rudies sandstone (Lower Miocene), Warda field, Gulf of Suez, Egypt. *J. Afr. Earth. Sci.* 66–67, 56–71. doi:10.1016/j.jafrearsci.2012.03.008
- Zaid, S. M. (2015). Geochemistry of sandstones from the Pliocene Gabir Formation, north Marsa Alam, Red Sea, Egypt: implication for provenance, weathering and tectonic setting. *J. Afr. Earth. Sci.* 102, 1–17. doi:10.1016/j.jafrearsci.2014.10.016
- Zhang, J. X., Xu, Z. Q., Xu, H. F., and Li, H. B. (1998). Framework of North Qilian Caledonian subduction accretionary wedge and its deformation dynamics. *Sci. Geol. Sin.* 33, 290–299.
- Zhang, J. X., Yu, S. Y., Li, Y. S., Yu, X. X., Lin, Y. H., and Mao, X. H. (2015). Subduction, accretion and closure of Proto-Tethyan Ocean: Early Paleozoic accretion/collision orogeny in the Altun-Qilian-North Qaidam orogenic system. *Acta Petrol. Sin.* 31, 3531–3554. [In Chinese with English abstract].
- Zhang, K., Liu, R., Bai, E., Zhao, Z. B., Peyrotty, G., Fathy, D., et al. (2023). Biome responses to a hydroclimatic crisis in an Early Cretaceous (Barremian–Aptian) subtropical inland lake ecosystem, Northwest China. *Palaeogeogr. Palaeoclimatol. Palaeoecol.* 622, 111596. doi:10.1016/j.palaeo.2023.111596
- Zhang, Q., Sun, X. M., and Zhou, D. J. (1997). The characteristics of North Qilian ophiolites, forming settings and their tectonic significance (in Chinese). *Adv. Earth Sci.* 12, 366–393.
- Zhang, T. S., Kershaw, S., Wan, Y., and Lan, G. Z. (2000). Geochemical and facies evidence for palaeoenvironmental change during the Late Ordovician Hirnantian glaciation in South Sichuan Province, China. *Glob. Planet. Change.* 20, 133–152. doi:10.1016/s0921-8181(99)00063-6
- Zheng, J. P., Griffin, W. L., Sun, M., O'Reilly, S. Y., Zhang, H. F., Zhou, H. W., et al. (2010). Tectonic affinity of the west Qinling terrane (Central China): North China or Yangtze? *Tectonics* 29, 339–341. doi:10.1029/2008tc002428
- Zhou, L., Algeo, T. J., Shen, J., Hu, Z. F., Gong, H., Xie, S., et al. (2015). Changes in marine productivity and redox conditions during the late Ordovician Hirnantian glaciation. *Palaeogeogr. Palaeoclimatol. Palaeoecol.* 420, 223–234. doi:10.1016/j.palaeo.2014.12.012
- Zhou, Y. Y., Zhao, T. P., Wang, C. Y., and Guo, H. H. (2011). Geochronology and geochemistry of 2.5 to 2.4Ga granitic plutons from the southern margin of the North China Craton: implications for a tectonic transition from arc to post-collisional setting. *Gondwana Res.* 20, 171–183. doi:10.1016/j.gr.2011.03.004
- Zou, C. N., Qiu, Z., Poulton, S. W., Dong, D. Z., Wang, H. Y., Chen, D. Z., et al. (2018). Ocean euxinia and climate change double whammy drove the late ordovician mass extinction. *Geology* 46, 535–538. doi:10.1130/g40121.1
- Zuo, G., and Liu, J. (1987). The evolution of tectonic of early Paleozoic in North Qilian range, China. *Sci. Geol. Sin.* 1, 14–24. [In Chinese with English abstract].
- Zuo, G. C., and Wu, H. Q. (1997). A subduction-collision orogenic model of Early-Paleozoic in the middle part of North Qilian area. *Adv. Earth Sci.* 12, 315–322. [In Chinese with English abstract].